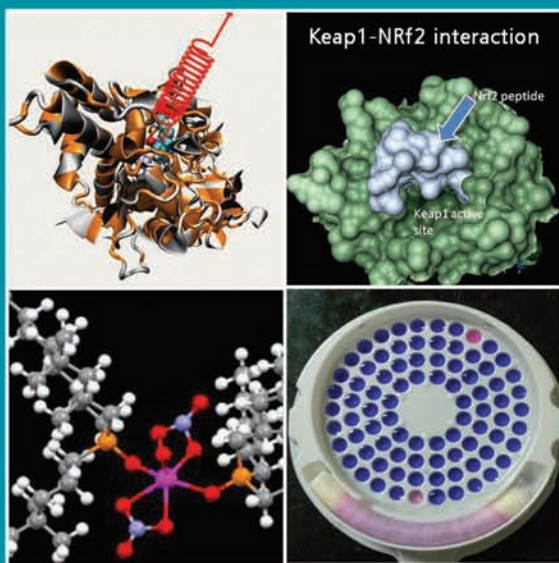


# BARC

## NEWSLETTER



### IN THIS ISSUE

- Estimation of Shutdown Reactivity in Power Reactor: Comparative Study of Inverse Point Kinetics and Kalman Filtering
- Understanding of Ternary Fission in Heavy-ion Induced Reactions
- Ultrasonic Phased Array Examination for BWR Pressure Vessel
- Fuel Handling System Training Simulator for 540 MWe PHWR
- ANUPAM-Adhya Supercomputer
- Biosensors for Environmental and Clinical Monitoring
- Groundwater Contamination Problems in Rural India: Detection and Remediation at the Household Level



## In the Forthcoming Issue

1. **Frontiers in Science & Cutting Edge Technologies:  
Physics Group in BARC**  
S. Kailas
2. **Development and Fabrication of LEU Plate Fuel for Modified Core of  
APSARA Reactor**  
P. V. Hegde et al.
3. **Metal Oxide Nanowires for Gas Sensing Application**  
N. Ramgir et al.
4. **Photocatalytic Hydrogen Generation from Water using Solar  
Radiation**  
R. Sasikala and S.R. Bharadwaj
5. **Development of Carbon/Carbon Composites for Nuclear  
Reactor Applications**  
Ramani Venugopalan et al.
6. **Searching for the Proverbial Needle in a Haystack:  
the Information Dilemma**  
Sangeeta Deokattey and K. Bhanumurthy
7. **VBMC: A Formal Verification Tool for VHDL Programs**  
Ajith K. John et al.

# Contents

<i>Editorial Note</i>	ii
<b>Brief Communication</b>	
• Periscope for In-Service Inspection of PFBR	iii
• Four-Piece Servo Manipulator	iv
• Single Photon Emission Computed Tomography for Nuclear Applications	v
• TPLC – 32: Trombay 32 bit Programmable Logic Controller Platform	vi
<b>Research Articles</b>	
• Estimation of Shutdown Reactivity in Power Reactor: Comparative Study of Inverse Point Kinetics and Kalman Filtering <i>T.U. Bhatt, S.R. Shimjith and A.P. Tiwari</i>	1
• Understanding of Ternary Fission in Heavy-ion Induced Reactions <i>Y.K. Gupta, R.K. Choudhury and A. Chatterjee</i>	6
<b>Technology Development Articles</b>	
• Ultrasonic Phased Array Examination for BWR Pressure Vessel <i>N. Jothilakshmi, P.P. Nanekar and B.K. Shah</i>	11
• Fuel Handling System Training Simulator for 540 MWe PHWR <i>Vinaya Kumar</i>	20
<b>Feature Articles</b>	
• ANUPAM-Adhya Supercomputer <i>K. Rajesh, K. Bhatt, D.D. Sonvane, K. Vaibhav, V. Duggal, U. Karnani, N. Chandorkar, K.R. Koli, R.S. Mundada and A.G. Apte</i>	27
• Biosensors for Environmental and Clinical Monitoring <i>Jitendra Kumar and S. F. D'Souza</i>	34
• Groundwater Contamination Problems in Rural India: Detection and Remediation at the Household Level <i>S.C. Chaurasia, A.C. Sahayam, G. Venkateswarlu, S.M. Dhavile, S. Thangavel, L. Rastogi and T. Mukherjee</i>	39
<b>News and Events</b>	
• DAE-BRNS 11 <sup>th</sup> Biennial Trombay Symposium on Radiation & Photochemistry (TSRP-2012): A Report	46
• Towards Smarter and Greener Flow Measurement and Control: A Report of the Global Conference and Exhibition	48
• DAE-BRNS Symposium on Emerging Trends in Separation Science and Technology (SESTEC-2012): A Report	49
<b>BARC Scientists Honoured</b>	

**Editorial Committee****Chairman**

Dr. Tulsi Mukherjee,  
Director, Chemistry Group

**Vice Chairman**

Dr. N. Ramamoorthy,  
Senior Advisor to Director, BARC

**Edited by**

Dr. K. Bhanumurthy  
Head, SIRD

**Associate Editors for this issue**

Dr. A.P. Tiwari, RCnD  
Dr. D.N. Badodkar, DRHR

**Members**

Dr. Tulsi Mukherjee  
Dr. N. Ramamoorthy  
Mr. C.S.R. Prasad, ChTD  
Dr. D.N. Badodkar, DRHR  
Dr. A.P. Tiwari, RCnD  
Dr. Madangopal Krishnan, MSD  
Dr. A.K. Tyagi, CD  
Dr. P.V. Varde, RRS  
Dr. S.M. Yusuf, SSPD  
Mr. Avaneesh Sharma, RED  
Dr. C. Srinivas, PSDD  
Dr. G. Rami Reddy, RSD  
Dr. S.K. Mukherjee, FCD  
Mr. G. Venugopala Rao, APPD  
Dr. A. Vinod Kumar, EAD  
Dr. Anand Ballal, MBD  
Dr. K. Bhanumurthy, SIRD  
Dr. S.C. Deokattey, SIRD

***From the Editor's Desk* .....**

You have with you the first issue of the BARC Newsletter for the year 2012 with its new front cover.

From this year, we have introduced a novel feature "Brief Communication". Every issue hence forth, will carry a one page write-up on the latest R&D, technological innovation being done at BARC. All BARC Scientists and Engineers are invited to send in their write-ups to any of the members of the Editorial Committee. The format and other details are available at the SIRD Divisional website under the hyperlink "Request Forms".

We welcome your comments and suggestions for further improving the quality of the BARC Newsletter.

**Dr. K. Bhanumurthy**  
On behalf of the Editorial Committee

## Periscope for In-Service Inspection of PFBR

A Periscope for in-service visual inspection of PFBR internals in the cover gas region has recently been developed. The Periscope is designed to operate at ambient temperature of 150° C and radiation field of 1.3 R/hr. This 10 m long Periscope has a diameter of 400 mm and is designed to provide a viewing resolution of 0.2 mm lines separated by 0.5 mm at a distance of 4 m from the objective end.

The Periscope provides facilities for image scanning in vertical plane, zooming, focusing and axial rotation. It also has inbuilt illumination system along with a light directing mechanism. The facilities of scanning, zooming, focusing, axial rotation and light direction are motorized and all the motors are housed within the Periscope. The Periscope can be operated either from the operator cabin housed above the Periscope or remotely from the main control panel. The facility for simultaneous viewing through one eyepiece and video recording through another eyepiece has also been incorporated in the design.

The Applied Spectroscopy Division, Centre for Design & Manufacture, Division of Remote Handling and Robotics, Glass & Advanced Ceramics Division and Technical Services Division from BARC along with IGCAR were involved in the design and fabrication of the Periscope. The periscope has recently been handed over to BHAVINI.

- Input received from Design, Manufacturing & Automation Group (DM&AG)



PFBR Periscope

## Four-Piece Servo Manipulator

The Nuclear industry employs many types of general-purpose remote handling tools for handling objects in radioactive environments. Master Slave Manipulators (MSMs) are the most versatile among them. BARC has developed many models of mechanical MSMs and installed them in various nuclear installations. A few models of electrically controlled servo manipulators were also developed. Continuous efforts are being put in to improve the quality of teleoperation. BARC has recently developed a novel design of Servo Manipulator, called Four-Piece Servo Manipulator (FPSM).

FPSM consists of a master arm and a slave assembly. The modular slave assembly has three distinct parts: a slave arm in the hotcell, a through-tube in the cell wall and a motor unit in the operating area. The motor unit of the slave assembly has eight motors for driving five rotary joints, two coaxial telescopic joints and a gripper. Operator can control the slave gripper in the hot cell, by manipulating the master arm handgrip in the operating area. When the operator moves the master arm, the controller drives the slave motors, based on the sensor inputs from

the master joints. Motor motions are transmitted to the slave arm and modified to the desired form, using a series of mechanical linkages. The 20-kg capacity manipulator has a maximum reach of 3.8 m.

The unique feature of FPSM is that, it can be installed in hotcells that are designed for mechanical MSMs: any telescopic mechanical MSM can be replaced by the FPSM. The operator-friendly FPSM has a few advantages over the conventional manipulators. Its slave arm is remotely replaceable. Its through-tube is sealed to prevent leakage of contamination from the hotcell. FPSM has low effective friction and reflects only a controlled load to the operator. Electric components of FPSM are not subjected to radiation damage or contamination, as they are kept outside the hotcell. They are also easily accessible for maintenance. In addition, the presence of computer in the control loop enables the operator to modify the input-output relations as required.

*- Input received from Design, Manufacturing & Automation Group (DM&AG)*



Four-Piece Servo Manipulator and its components

# Single Photon Emission Computed Tomography for Nuclear Applications

For many of the applications in nuclear fuel cycle, it is important to know the distribution of nuclear material in a bulk matrix. For example, fission product distribution in a fuel bundle is required for burnup estimation. Similarly, at the back end of nuclear fuel cycle, distribution of nuclear materials in nuclear waste drum is required for its safe disposal and nuclear material accounting. For these applications not only the positional information of the distribution of nuclear material is needed but also its source strength. Emission tomography is one of the important methods for such characterization.

SPECT (Single Photon Emission Computed Tomography) provides for an invaluable non-invasive technique for the characterization and activity distribution of the gamma-emitting source. SPECT involves the position-sensitive measurement of gamma rays emitted by a radionuclide. The intensities of the radiation measured are directly related to the radionuclide distribution inside the object.

We have developed SPECT system for scanning waste drums at Purnima Labs. For SPECT imaging

of radioisotopes, Active and Passive Computed Tomography (A&PCT) method has been employed. During the Active measurements, an external gamma source is used to determine the attenuation map of the object. With this knowledge of the attenuation map, the Passive measurements are then carried out by recording projection data at various angles over 360 degrees. These two data are then used to reconstruct the gamma sources inside the object.

The reconstruction step is basically finding the inverse of the Attenuated Radon Transform (Eq.1)

$$g(\theta, s) = (R_{\mu} f)(\theta, s) = \int_{-\infty}^{\infty} f(s\underline{\theta} + t\underline{\theta}^{\perp}) e^{-(D_{\mu})(s\underline{\theta} + t\underline{\theta}^{\perp} \cdot -\underline{\theta}^{\perp})} dt \tag{1}$$

An analytical solution for the attenuated Radon Transform was provided by Novikov (known as the Novikov's Inversion Formula (Eq.2))

$$f(\underline{x}) = \frac{1}{4\pi} \text{Re} \left\{ \nabla \cdot \int_0^{2\pi} \underline{\theta} \left\{ e^{-h(\theta, s) + (D_{\mu})(\underline{x} \cdot -\underline{\theta}^{\perp})} H e^{h(\theta, s)} g(\theta, s) \right\} \Big|_{s=\underline{x} \cdot \underline{\theta}} d\theta \right\} \tag{2}$$

- Input received from Physics Group (PG)

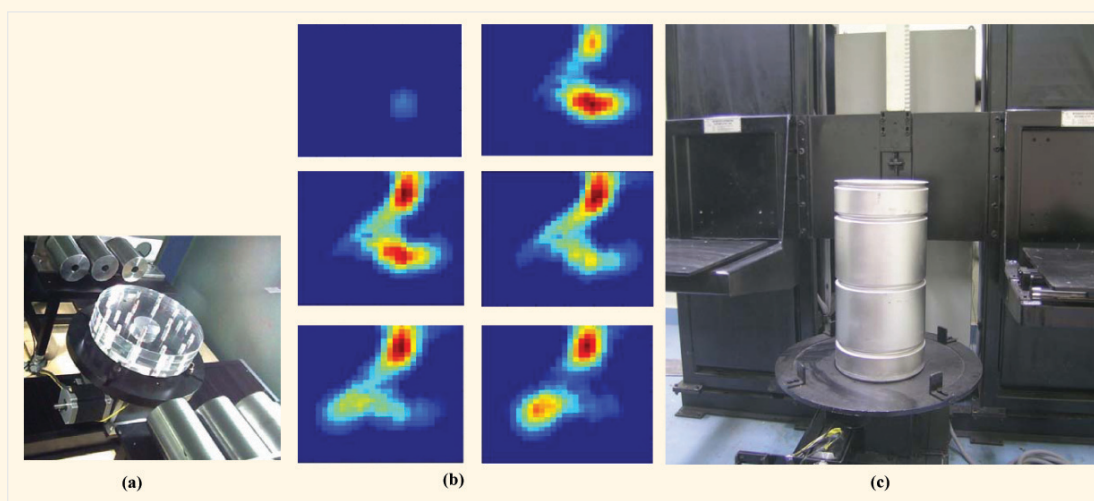


Fig. (a) Prototype lab-based experimental set-up (b) six XY-sectional views of 3D Reconstructed activity of Cs-137 sources in perspex matrix (Three distinct source locations can be observed) (c) Full-scale experimental set-up at Purnima Labs for scanning waste drum

## TPLC – 32: Trombay 32 bit Programmable Logic Controller Platform

Emerging trend the world over is to use qualified configurable platform to design and deploy safety and safety related C & I systems in nuclear reactors and other nuclear facilities. The platform-based design provides complete configurability, such that it can be used to build different systems for diverse applications. This approach offers several benefits, e.g., it renders ease in system development and reduces system qualification efforts. Incorporating modifications to the system, if necessary after installation in the plant, is also done with much less effort.

Keeping up with the current trend, Qualified TPLC-32 Platform has been developed by Electronics and Instrumentation Group, especially to implement safety and safety related systems requiring deterministic behavior, fault-tolerance and conformance to pertinent codes and guides. The Verification and Validation (V&V) of TPLC-32 Platform has been carried out by an independent team of engineers.

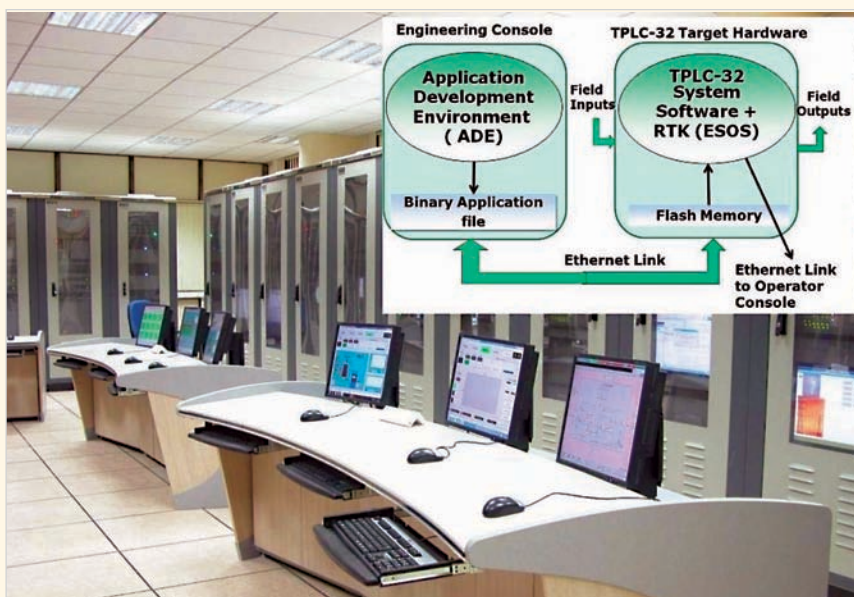
The TPLC-32 hardware consists of *inhouse* developed single board computer having 32 bit processor and intelligent I/O boards and Ethernet boards. An Engineering Console (EC) can be linked to TPLC-32 hardware over Ethernet interface. The Application Development Environment (ADE) software on the EC is used to configure, test, build and download applications, which the TPLC-32 embedded system software executes under the control of ESOS – an *inhouse* developed Real Time Kernel.

ADE in TPLC – 32 has several programmable features, some salient ones being Process logics, control schemes and interlocks in the form of Function Block diagrams and Library of 61 function blocks comprising logical, arithmetical, timer, counter, comparison and process control functions.

Some C&I systems have been successfully developed using TPLC-32 Platform and are being deployed in nuclear reactors and installations while some implementations are in progress. Complete in-house

design with associated documentation assures long term support, scalability and solutions in tune with continuous changes in technology.

- Input received from  
Electronics &  
Instrumentation Group  
(E&IG)



TPLC-32 based Distributed C&I System for a nuclear installation (In the inset, the context-diagram of TPLC – 32 is shown)



# Estimation of Shutdown Reactivity in Power Reactor: Comparative Study of Inverse Point Kinetics and Kalman Filtering

T.U. Bhatt, S.R. Shimjith and A.P. Tiwari  
Reactor Control Division

## Abstract

Measurement and on-line display of reactivity are of great help in calibration of reactivity control and safety devices and planning of suitable actions during the reactor operation. Reactivity can be estimated by the traditional Inverse Point Kinetics (IPK) method or by a recently developed Kalman filtering (KF) based method. The KF based reactivity estimation proves superior to IPK method, especially in subcritical operating regime which is characterized by very low neutron flux level and large fluctuations in it.

In this article, a comparison in the performance of the reactivity estimation by methods based on KF and IPK has been made by analysis of data collected from power reactors. The KF based approach has been found to yield higher accuracy, noise suppression and robustness than IPK based approach.

## Introduction

On-line measurement and indication of reactivity in a nuclear reactor are very much important from the points of view of monitoring shutdown margin, calibration of safety and control devices, detection of any inadvertent introduction of reactivity into the core, quantification of the worth of fuel bundles, imposing restrictions on reactivity range of control etc. The reactivity meter facilitates continuous surveillance of the core reactivity status from shutdown through the start-up and power range operation of the reactor. It provides the operator with a direct indication of the net reactivity, which is a much more definitive indication of the status of the core than other parameters such as the power and log rate do.

Many modern reactors are equipped with on-line reactivity meters, which mainly employ techniques like inverse point kinetics (IPK). However, this technique suffers from some serious drawbacks like high sensitivity to reactor parameters and less immunity to noise content in the input signals, hence effective only during power range operation. An on-line reactivity meter based on Kalman Filtering

Technique can be used for direct indication of the core reactivity status under critical as well subcritical operating regimes of a nuclear reactor [1]. The Kalman filter based algorithm can work in noisy environment and modeling errors and uncertainties in parameters do not affect the estimation severely as the feedback gain is continuously adjusted during the estimation process. In this article, its performance has been compared with IPK approach for estimation of shutdown reactivity from power variation data sets recorded in power reactors.

## Methods of Reactivity Estimation

The measurement of reactivity can be made in an indirect way only. It must be deduced from the observation of neutron flux density/power which is caused by reactivity. In the following, IPK and Kalman filtering techniques of measuring reactivity are discussed. Both the techniques rely upon the point kinetics model of a nuclear reactor, expressed as

$$\frac{dP}{dt} = \left( \frac{\rho - \beta}{\ell} \right) P + \sum_{i=1}^m \lambda_i C_i + S \quad (1)$$

$$\frac{dC_i}{dt} = \frac{\beta_i}{\ell} P - \lambda_i C_i, \quad i = 1, 2, \dots, m \quad (2)$$

where  $P$  denotes the reactivity,  $P$  denotes the neutronic power,  $C_i$  the concentration of the  $i^{\text{th}}$  group of delayed neutron precursor and  $m$  is the total number of delayed neutron precursor groups,  $\beta_i$  and  $\lambda_i$  are delayed neutron parameters,  $\ell$  denotes the prompt neutron life time and  $S$  denotes a neutron source.

### Estimation Based on Inverse Point Kinetics (IPK)

From the point kinetics model, the following equation can be derived [1, 2]:

$$\rho = \frac{\ell}{P} \left[ \frac{dP}{dt} + \sum_{i=1}^m \frac{dC_i}{dt} - S \right] \quad (3)$$

In general it is convenient to treat discrete dynamic models instead of continuous ones because quantities that come from real observations are discrete. Suppose the samples of neutronic power (measurement) are available as  $P_k$  at time instant  $kT$ ,  $k=0,1,2,\dots$ , where  $T$  is sampling interval. Then from (2)

$$C_{i,k} = e^{-\lambda_i T} C_{i,k-1} + \frac{1}{\lambda_i} (1 - e^{-\lambda_i T}) \frac{\beta_i}{\ell} P_k \quad (4)$$

Further in (3) the derivative can be approximated as

$$\left. \frac{dP}{dt} \right|_k = \frac{P_k - P_{k-1}}{T} \quad \text{and} \quad \left. \frac{dC_i}{dt} \right|_k = \frac{C_{i,k} - C_{i,k-1}}{T} \quad (5)$$

and thus

$$\rho_k = \frac{\ell}{P_k} \left[ \frac{P_k - P_{k-1}}{T} + \sum_{i=1}^m \frac{C_{i,k} - C_{i,k-1}}{T} - S \right] \quad (6)$$

which is suitable for implementation on a digital computer and it will give estimate of reactivity at different time instants.

When fluctuations in neutron flux are large, such as in highly subcritical regime, the reactivity estimate would be accordingly very noisy. This method does not have any effective provision for noise elimination. Hence it is difficult to calculate reactivity using IPK in subcritical operating regime where neutron flux level is quite low and fluctuation of the neutron signal is very large.

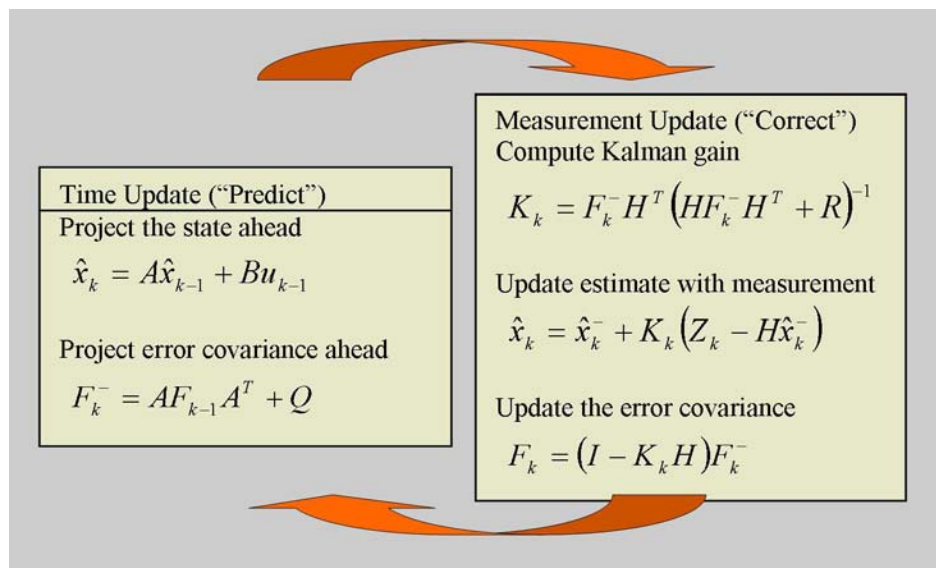


Fig. 1: Kalman Filter Algorithm

**Estimation Based on the Kalman Filtering (KF) Technique**

The Kalman filter is a predictor-corrector type state estimator that is optimal in the sense that it minimizes the estimated error covariance when some presumed conditions are met. The equations for the Kalman filter fall into two groups: time update equations (predictor equations) and measurement update equations (corrector equations). The time update equations are responsible for projecting forward (in time) the current state and error covariance estimates to obtain the a priori estimates for the next time step. The measurement update equations are responsible for the feedback i.e. for incorporating a new measurement into the a priori estimate to obtain an improved a posteriori estimate. The Kalman filter algorithm is summarized in Fig. 1. [3].

Where  $x$  is state variable, vector,  $A$  is state transition matrix,  $B$  is input matrix,  $H$  is output matrix,  $F$  is state error covariance matrix,  $K$  is Kalman gain,  $Z$  is measurements,  $Q$  is process noise covariance and  $R$  is measurement noise covariance.

The estimation of reactivity based on Kalman filtering requires mathematical model consisting of first order differential equations for neutron flux density/power and delayed neutron precursors' concentrations i.e. (1) and (2). In addition, equations for reactivity variation are required. In a nuclear reactor, reactivity variations can be described as white noise with zero mean and nonzero covariance. Then it is possible to write

$$\frac{d\rho}{dt} = \omega \tag{7}$$

and

$$\frac{d\omega}{dt} = 0 \tag{8}$$

These equations are cast in standard state space form, discretized to obtain the matrices  $A$  and  $B$  and are solved recursively for predicting the reactivity alongwith reactor power, delayed neutron precursor concentrations etc [1, 4]. The predicted value of

the reactor power is compared with the measured reactor power, and each of the predicted parameters is corrected by applying the deviation between the two through an optimal feedback gain. This prediction-correction algorithm claims weightage over the IPK mainly in terms of insensitivity to reactor parameters. Moreover, the Kalman Filtering technique, being a stochastic estimator, has inherent capability to handle process and measurement noise. This feature also makes the algorithm more suitable for estimation of reactivity under highly subcritical conditions where the signal to noise ratio is poor.

**Analysis of Power Variation Data and Results**

The reactivity has been estimated from the data sets collected from power reactors in three different cases. In each case the value of reactivity estimated using the KF technique is compared with the estimate obtained using IPK technique. In the following, results are presented for each case. The values of different neutronic parameters used in analysis are given in the table below:

Group (i)	Decay Constant ( $\lambda_i$ ), $s^{-1}$	Fractional Yield $\beta_i (\times 10^{-3})$
1	0.0120	0.2487
2	0.0317	1.3800
3	0.1183	1.1990
4	0.3101	2.6270
5	0.9617	1.3790
6	2.8930	0.6799
Total		7.5127

Value of prompt neutron life time ( ) is taken as  $9.2939 \times 10^{-4} s$ .

**Low Power Reactor Trip by Primary Shutdown System (PSS)**

Initially the reactor was maintained in a critical condition at a very low power level of approximately 0.08 %FP. Then shut off rods were dropped by actuating trip. The data was recorded at uniform interval of 10 ms for 5 seconds. Variation in power

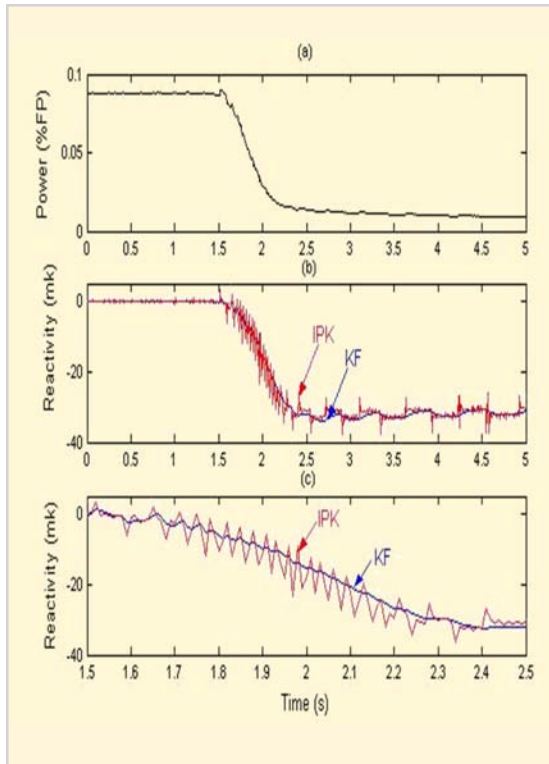


Fig.2: Variation of reactor power and estimated reactivity in trip by Shut off rods drop

signal is shown in Fig. 2(a). The reactivity estimation based on the Kalman filtering technique and IPK are plotted in Fig. 2(b). A zoomed view of Fig. 2(b) is also shown in Fig. 2(c) for clear comparison. It is evident from Fig. 2(b) and Fig. 2(c) that IPK yields a comparable reactivity, but with very large noise content. Thus Kalman filter perform better than IPK does.

### Low Power Reactor Trip by Secondary Shutdown System (SSS)

In this case, initially the reactor was maintained in a critical condition at a very low power level of 0.08 % FP, and then SSS was actuated at 1.54 s. The data was recorded uniformly at 10 ms interval for 5 seconds. The variations in reactor power and estimated reactivity are plotted in Fig. 3. It is observed that the reactivity estimated by Kalman filter algorithm is in very close agreement with the IPK estimation. The Kalman filter gives smoother estimation of reactivity as compared to IPK.

### Reactor Trip and Start up

Fig. 4(a) shows variation in reactor power for reactor trip followed by restart and afterward long shutdown. The data were recorded at uniform intervals of 1 s for 45 minutes. Initially the reactor was operating in a critical condition at power level of approximately 85 %FP. The setback and trip were actuated at 43 s and 60 s respectively, followed by reactor reset. Subsequently power was raised to approximately 60 %FP. Then again setback and trip were actuated at 1622 s and 1665 s respectively and afterward reactor was remaining in shutdown state. The estimated reactivity based on Kalman filtering and IPK are plotted in Fig. 4(b). It is observed from Fig. 4(b) that estimated reactivity reaches to -30 mk during reactor trip and afterward estimated reactivity become slightly positive of the order of 0.5 mk at 1000 s as reactor was reset and power was being raised. Then followed by reactor trip subcriticality

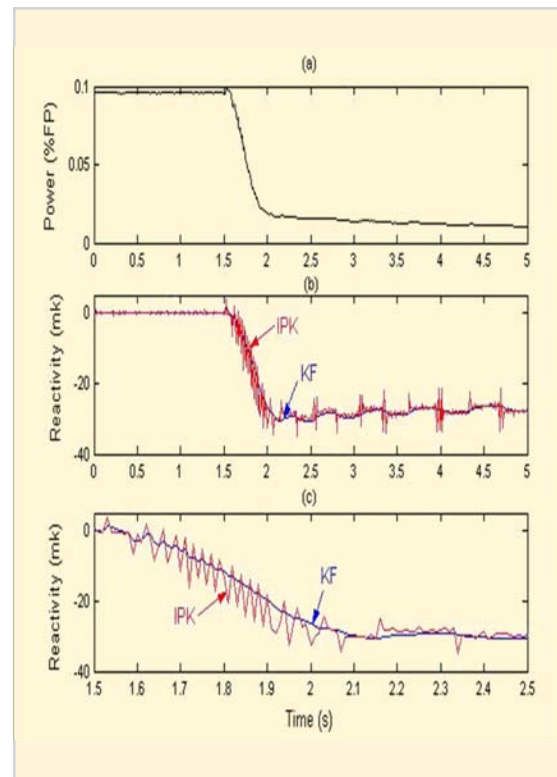


Fig. 3: Variation of reactor power and estimated reactivity during SSS Actuation

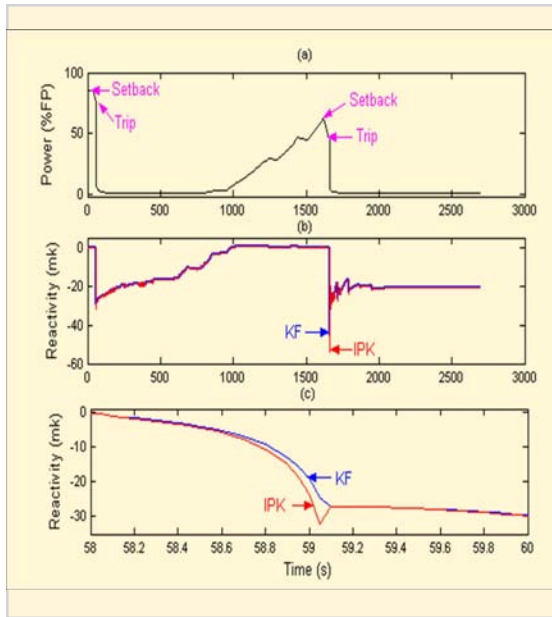


Fig. 4: Variation of reactor power and estimated reactivity during reactor operation

reaches a peak value of  $-45\text{ mk}$  (based on KF) and to  $-52\text{ mk}$  (based on IPK) and subsequently the reactivity stabilizes at around  $-22\text{ mk}$ . There is a large undershoot in the estimated reactivity based on Kalman filtering and IPK techniques, although IPK give a more undershoot compared to Kalman filtering.

**Conclusions**

A comparative study of reactivity estimation methods based on IPK and KF has been done in this article by analysis of data collected from a PHWR. The reactivity estimation is effectively obtained in transient involving trip/shutdown and startup. It is found that, in comparison to IPK technique, Kalman

filtering technique for reactivity estimation is superior in all cases considered. Specifically, noise contents and undershoot in estimated reactivity are extremely less with Kalman filtering technique. The subcriticality state is inferred in unambiguous manner for several minutes after reactor shutdown.

In a power producing thermal reactor, where xenon feedback effect is strong, Kalman filtering technique can be used to show the subcriticality margin at any time after trip or shutdown whereby operations like addition of boron in moderator and restart up can be planned.

**References**

1. A.P. Tiwari, B.R. Ivan. "Kalman Filtering Technique for Reactivity Measurement". Proceedings of symposium on Advances in Nuclear and Allied Instrumentation (SANAI - 97), Feb 5-7, 1997, BARC.
2. Saleem A. Ansari, "Development of Online Reactivity Meter for Nuclear Reactor," *IEEE Transactions on Nuclear Science*, 38, (4), 946 - 952 (August 1991).
3. H. W. Sorenson, "Kalman Filtering Techniques," Kalman Filtering: Theory and Application, edited by H. W. Sorenson, New York: IEEE Press, 90 - 126 (1985).
4. Attila Racz, "On the Estimation of a Small Reactivity Change in Critical Reactors by Kalman Filtering Technique," *Ann. Nucl. Energy*, 19, (9), 527 - 538 (1992).

# Understanding of Ternary Fission in Heavy-Ion Induced Reactions

Y.K. Gupta, R.K. Choudhury and A. Chatterjee

Nuclear Physics Division

## Abstract

The alpha particle energy spectra have been measured in coincidence with fission fragments over a wide range of relative angles with respect to fragment emission direction in  $^{11}\text{B}$  (62 MeV) +  $^{232}\text{Th}$  reaction. The ternary fission component was extracted using the moving source model analysis. The obtained results along with available literature data over a wide range of fissility and excitation energy of compound system have been analyzed to develop certain global features of the ternary fission. It is seen that in heavy-ion induced fission reactions, the ternary emission of alpha particles is a statistical process in contrast to the dynamical one as observed in spontaneous and thermal neutron induced fission. This indicates that the neck collapse is faster in case of low-energy or spontaneous-fission whereas at higher excitation energy, it is a slow process.

## Introduction

The discovery of nuclear fission by Hahn and Strassmann in 1939 paved the way for unfolding a vast reserve of energy for mankind. The phenomenon of nuclear fission came as a big surprise, as it was quite difficult to imagine in those days that a uranium nucleus with total binding energy of about 2000 MeV could split into two parts with the impact of a slow neutron. It appeared as if a giant rock could fall apart with the impact of a light feather. Nuclear fission emerged as a beautiful gift to society in the form of sustained nuclear energy production. Soon after the discovery of nuclear fission, world's first nuclear energy reactor, Chicago Pile-1 (CP-1, USA) was built, where a self-sustaining nuclear chain reaction was initiated on December 2, 1942.

In addition to energy production, fission process itself is the most classic example of complex nuclear dynamics involving large scale collective motion in nuclear physics. Since discovery, it has been challenging for chemists as well as physicists to understand the mechanism of nuclear fission. The fission process provides a laboratory within which one can study the interplay between macroscopic aspects of the nuclear bulk matter and microscopic

effects of the finite number of Fermions. Moreover, simultaneous manifestation of both statistical and dynamical effects makes the fission process more appealing.

During the fission process, the nuclear many-body system evolves through a large scale rearrangement of the nucleons and subsequently divides into two fragment nuclei. The splitting of a nucleus into two fission fragments is termed as binary fission. The fission process is basically governed by the characteristic features of the fission barrier present in the map of potential energy versus deformation of a nucleus [1]. The maximum of the potential energy with respect to ground state is the height of fission barrier. Although the fission barrier height is much smaller than the total energy released in fission, it is the fission barrier which controls the fission process. The fission barrier height decreases as  $Z^2/A$  of the fissioning nucleus increases. The spontaneous fission half-life therefore, decreases exponentially with increasing  $Z^2/A$  [1]. There are two landmark points during the fission process: saddle point and scission point. In the potential energy map, the fission barrier point is known as the saddle point. The scission point represents that stage of

the process where the nascent fragments are in just touching configuration and are about to fly away in each other's Coulomb field.

At the time of scission, the possibility of splitting of a nuclear stretched configuration into three parts was initiated in 1941. The first experimental evidence for fission not into two, but into three fragments was observed from fission tracks in nuclear emulsions. This type of fission where a third particle is emitted along with the two fission fragments is known as ternary fission. Detailed investigations have been carried out in low energy ternary fission (spontaneous, thermal neutron, and photo-fission) and are well documented in various review articles [2,3]. These investigations show that 90% of ternary particles are the  $\alpha$ -particles which are also called as long range alphas (LRA) in order to differentiate from less energetic alphas from radioactive decays. Other particles such as, tritons, deuterons, and protons have significantly lower probability of emission in

ternary fission [2].

### Ternary Fission Characteristic

From low energy fission experiments it is observed that the ternary charged particles exhibit characteristic energy and angular distributions resulting from strong focusing of the particles by the Coulomb forces of the nascent fission fragments [3-6] and it is concluded that ternary particles are generated close to scission (rupture) point between the main two fission fragments. Ternary fission thus often referred as near scission emission (NSE). The angular distribution of these NSE  $\alpha$  particles is Gaussian in shape and peaks around perpendicular to the scission axis. The energy distribution is also Gaussian and peaks between 15 to 16 MeV for all the fissioning nuclei. The near-scission  $\alpha$ -particle multiplicities ( $\alpha_{nse}$ ) are found to increase linearly with  $Z^2/A$  of the fissioning system. These features of the NSE observed in low energy fission have been

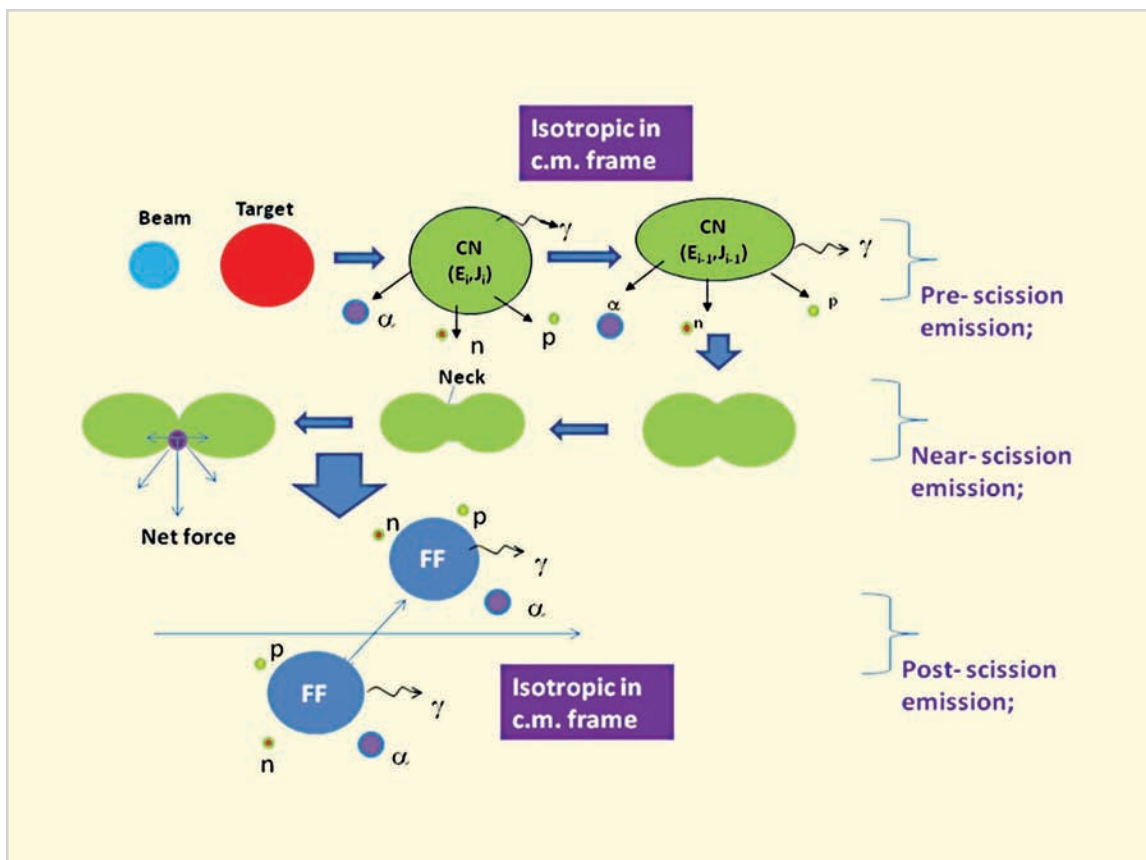


Fig. 1: Different stages of particle emission in heavy-ion induced fusion-fission reaction.

understood qualitatively within the framework of a dynamic model suggested by Halpern [3]. In this model, it is assumed that at the time of scission, the neck joining the two nascent fragments collapses suddenly and the emitted particle gains energy from the rapidly changing nuclear potential.

In the low excitation energy regime, the near scission emission is the dominant mode of the particle emission, whereas in heavy-ion induced fission it can take place at various stages, namely, from the fissioning compound nucleus (pre-scission), from the accelerated fission fragments (post-scission), and the NSE [7-10] as depicted in the Fig.1. In heavy-ion induced fission, the near scission  $\alpha$ -particle emission has been studied only for a limited number of target-projectile systems due to the complexity of measurements and the analysis procedure [7-10]. From the available heavy-ion data, it has not been possible to explain the emission mechanism near the scission configuration over a large fissility ( $x$ ) and excitation energy ( $E_{CN}$ ) range. The near scission emission is important to understand the scission point characteristics and the overall fission dynamics, as the features of this type of emission are decided by the saddle to scission dynamics.

We have started a program to extract the NSE component for a variety of compound nuclear systems employing different target projectile combinations to understand the NSE mechanism over a large range of  $x$  and  $E_{CN}$ . In this series we have started with the system  $^{11}\text{B}$  (62 MeV) +  $^{232}\text{Th}$  ( $Z^2/A=37.13$ ,  $x=0.798$ ) and carried out measurements of  $\alpha$ -particle energy spectra in coincidence with fission fragments in a wide range of relative angles between fission fragments and  $\alpha$ -particle emission [11]. The present results are analyzed along with other heavy-ion data from literature over a large  $x$  and  $E_{CN}$  range to understand the NSE mechanism.

### Experimental Details and Results

The experiments were performed using  $^{11}\text{B}$  beam of energy 62 MeV from the BARC-TIFR 14-MV Pelletron accelerator facility at Mumbai. A typical experimental

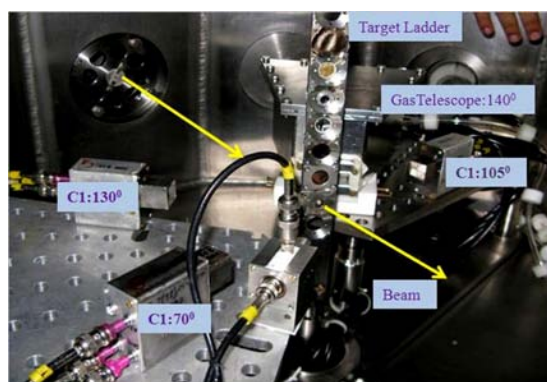


Fig. 2: Experimental setup.

setup is shown in Fig.2. The fission fragments were detected using a position sensitive 32-strip silicon detector [12] and a position sensitive gridded gas ionization chamber [13]. The  $\alpha$ -particles were detected using CsI(Tl)-Si(PIN) detectors. The particle identification in CsI(Tl) detectors was achieved using pulse shape discrimination (zero cross over) technique [14]. Using this technique, different radiations such as  $\gamma$ -rays, proton, deuteron, triton,  $\alpha$ -particles, and projectile like fragments (PLFs) are well separated as shown in Fig.3. A total number of twenty-four combinations of  $\alpha$ -particle spectra having different relative angles with respect to the beam ( $\theta_\alpha$ ) and fission fragments ( $\theta_{\alpha fd}$ ) were obtained. The normalized  $\alpha$ -particle multiplicity spectra were obtained by dividing the coincidence spectra with total number of fission single events.

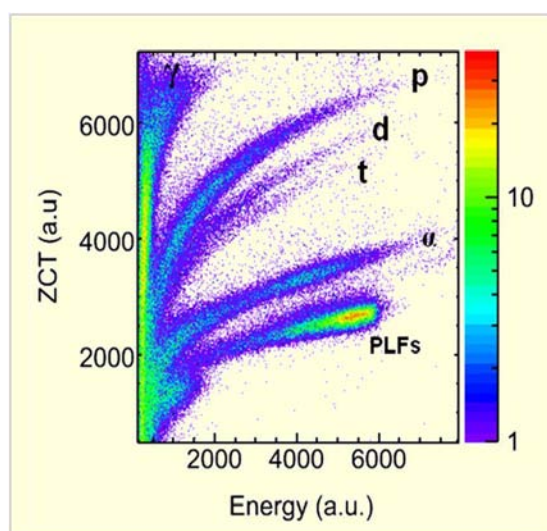


Fig. 3: Particle identification in CsI(Tl) detectors using Pulse Shape Discrimination (PSD) technique.



Each  $\alpha$ -particle multiplicity spectrum has contributions due to emission from four sources, namely the compound nucleus, NSE, and the two complementary fission fragments. All these twenty-four spectra are simultaneously fitted by the moving source model which utilizes kinematic focusing effect and different emission barriers for different sources [11]. The best fitted values of the multiplicity (number of  $\alpha$ -particles emitted per binary fission) corresponding to different stage of the particle emission are found to be  $\alpha_{pre} = (5.2 \pm 0.1) \times 10^{-3}$ ,  $\alpha_{post} = (0.17 \pm 0.02) \times 10^{-3}$ ,  $\alpha_{nse} = (0.5 \pm 0.05) \times 10^{-3}$ , corresponding to minimum  $\chi^2$  per degree of freedom value of 5.07.

### Near-Scission Multiplicity and Fission Dynamics

The value of  $\alpha_{nse}$  determined in the present work at  $E_{CN} = 45$  MeV, is observed to be significantly lower than the  $Z^2/A$  systematics of low excitation energy fission. There are a number of striking differences observed between the features of near-scission  $\alpha$ -particle emission in low energy fission and heavy-ion induced fission. In low excitation energy fission,  $\alpha_{nse}$  increases linearly as a function of  $Z^2/A$  of the fissioning system. As noted earlier, the low energy data can be explained by the liquid drop model calculations for dynamical emission of  $\alpha$ -particles

near the scission configuration, as the gain in potential energy from saddle to scission increases with  $Z^2/A$  [1, 2]. The peak energy for NSE  $\alpha$ -particles,  $\epsilon_p$  in low energy fission is constant within 15 to 16 MeV [1, 2] whereas in heavy-ion induced fusion-fission reactions it varies from 12.5 to 19.5 MeV for different systems [7-11,15,16]. In heavy-ion induced fusion-fission reactions it has been observed that  $\alpha_{nse}$  increases strongly with excitation energy [15] in contrast to low excitation energy fission, where dependence of the  $\alpha_{nse}$  on excitation energy in the range of 8 to 20 MeV is quite weak [1]. These comparisons about the features of NSE indicate that the near-scission emission mechanism in heavy-ion induced fission is different from low excitation energy fission.

In order to understand near scission emission mechanism in heavy-ion induced fusion-fission process, the ratio of  $\alpha_{nse}$  to the total pre-scission multiplicity ( $\alpha_{pre} + \alpha_{nse}$ ) for the present system along with other heavy-ion data from literature for different excitation energies has been plotted in Fig. 4 as a function of  $Z^2/A$ . It is seen that fraction of  $\alpha_{nse}$  is nearly same at around 10% of the total pre-scission multiplicity over a wide range of  $Z^2/A$  and excitation energy, as indicated with dashed lines in Fig. 4. The insensitivity of  $\alpha_{nse}$  with  $Z^2/A$  has been seen earlier also by Sowinski *et al.* [8] for two projectile-target systems having widely different values of  $Z^2/A$ . These features of  $\alpha_{nse}$  in heavy-ion induced fission indicate that  $\alpha$ -particles emitted from the neck region near the scission point are due to statistical emission process in contrast to low energy fission where it is a pure dynamical process [3]. It seems that as the available excitation increases, statistical emission dominates over dynamical emission. This indicates that the neck joining the nascent fission fragments collapses faster in low energy or spontaneous fission case [3], whereas at higher excitation energies it is a slow process. It is, therefore, inferred that the nuclear collective motion exhibits a change over from super-fluid to viscous behaviour with increase in excitation energy.

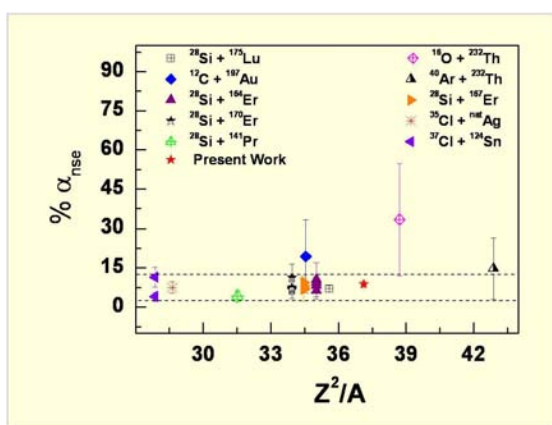


Fig. 4: The %  $\alpha_{nse}$  as a function of  $Z^2/A$  of the fissioning system. The different data points are for following systems:  $^{28}\text{Si} + ^{175}\text{Lu}$  [16],  $^{28}\text{Si} + ^{164,167,170}\text{Er}$  [15],  $^{37}\text{Cl} + \text{nat}\text{Ag}$  [9],  $^{40}\text{Ar} + ^{232}\text{Th}$  [10]. Data for  $^{37}\text{Cl} + ^{124}\text{Sn}$  and  $^{28}\text{Si} + ^{141}\text{Pr}$  are from Ref. [7] and for  $^{16}\text{O} + ^{232}\text{Th}$  and  $^{12}\text{C} + ^{197}\text{Au}$  are from Ref. [8]

## Conclusion

In the present article, we have carried out a systematic analysis for ternary alpha particle emission in heavy-ion induced fission reactions from the measurement in  $^{11}\text{B}$  (62 MeV) +  $^{232}\text{Th}$  reaction along with reported data in the literature. The fraction of ternary alpha particle multiplicity is observed to be nearly same at around 10% of the total multiplicity for various systems indicating that the ternary emission of alpha particles is a statistical process in heavy-ion induced fission reactions. This reveals that the neck collapse is faster in case of low-energy or spontaneous fission whereas at higher excitation energy, it is a slow process. It is, therefore, inferred that the nuclear collective motion exhibits a change over from super-fluid to viscous behaviour with increase in excitation energy.

## Acknowledgement

Authors are thankful to Dr. D.C. Biswas, B. K. Nayak, A. Saxena, B.V. John, K. Ramachandran, B. N. Joshi, L. S. Danu, K. Mahata, and S. K. Pandit for their help in various aspects of this work.

## References

1. R. Vandenbosch and J. R. Huizenga, Nuclear Fission (Academic, New York, 1973).
2. A.K.Sinha, D.M.Nadakarni, G.K.Mehata, *Pramana-J. Phys.* Vol.33, 85(1989).
3. I. Halpern, *Annu. Rev. Nucl. Sci.* 21, 245 (1971).
4. R. K. Choudhury et al. *Pramana-J. Phys.* Vol.6, 64(1976).
5. R. K. Choudhury et al. *Pramana-J. Phys.* Vol.8, 315(1977).
6. R. K. Choudhury and V. S. Ramamurthy, *Phys. Rev. C*18, 2213(1978).
7. B. Lindl, et al., *Z. Phys. A - Atmos and Nuclei* 328, 85 (1987).
8. M. Sowinski, et al., *Z. Phys. A - Atmos and Nuclei* 324, 87 (1986).
9. L. Schad, et al., *Z. Phys. A - Atmos and Nuclei* 318, 179 (1984).
10. K. Siwek - Wilczynska, et al., *Phys. Rev C* 48, 228 (1993).
11. Y. K. Gupta et al. *Phys. Rev C*84, 031603(2011).
12. R. P. Vind et al. *Nucl. Instr. and Meth. A* 580, 1435 (2007).
13. D. C. Biswas, et. al., *Nucl. Instr. and Meth. A* 340, 551 (1994).
14. Y. K. Gupta, et. al., *Nucl. Instr. and Meth. A* 629, 149(2011).
15. J. P. Lestone, et al., *Nucl. Phys. A* 559, 277 (1993).
16. K. Ramachandran, et al., *Phys. Rev C* 73, 064609 (2006).

# Ultrasonic Phased Array Examination for BWR Pressure Vessel

N. Jothilakshmi, P.P. Nanekar and B.K. Shah  
Quality Assurance Division

## Abstract

The reactor pressure vessel (RPV) of BWR at Tarapur is made from low alloy steel and is clad from inside with 308L austenitic stainless steel. The welds joint in the pressure vessel, both longitudinal and circumferential, are required to be inspected periodically for flaw detection and characterization. An ultrasonic phased array technique has been developed for in-service inspection of the circumferential weld joint between the RPV and top flange. The technique offers several benefits over the conventional ultrasonic testing methods. This article gives details of the simulation study carried out for arriving at the phased array inspection parameters and discusses the experimental results obtained on the mock-up. It is planned to use this technique for in-service inspection of the weld joint during the forthcoming re-fuelling outage scheduled in July 2012 at the plant site.

## Introduction

The BWR Reactor Pressure Vessel (RPV) at Tarapur Atomic Power Station (TAPS) is made from 120 mm thick low alloy steel. The vessel is clad from inside surface with 308L austenitic stainless steel. As per the requirements of ASME B&PV Code Sec XI, the pressure vessel welds are required to be examined periodically during in-service inspection. The RPV at TAPS has four circumferential welds and six longitudinal welds. Currently, only the top circumferential weld (C1) and two longitudinal welds (not shown in Fig. 1) are accessible for in-service inspection. The remaining welds are not accessible for any examination due to biological shield on the outside surface and core internals on the inside surface. The C1 weld is a weld joint between the RPV shell and the top flange (Fig. 1). This weld can be examined from ID surface by ultrasonics but previous attempts to do so did not yield satisfactory results due to rough surface of the clad. Due to these limitations, the examination of C1 weld was attempted from the top surface of the flange. The examination involved normal beam testing using a conventional probe. The top flange has many penetrations for fixing the bolts. As a result 100% examination of the weld joint could not be carried

out using the conventional ultrasonic method.

Ultrasonic phased array technique has been developed at Quality Assurance Division (QAD),

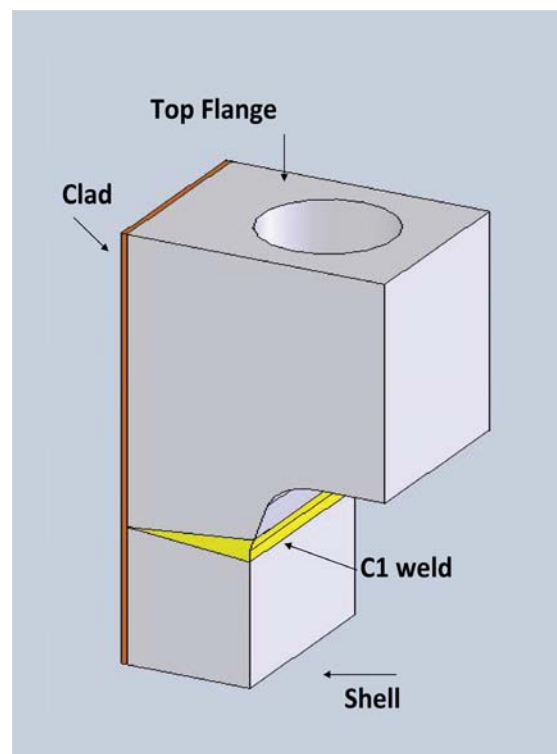


Fig. 1: C1 weld in RPV

BARC to examine the C1 weld joint in RPV of BWR at TAPS. Unlike conventional ultrasonics, phased array uses an array of sensors, which can be fired in a programmable manner. By altering the firing sequence and the delay in firing these sensors the user can manipulate the sound beam inside the component under inspection. These manipulations can be of several forms such as electronic scanning, multiple-angle scanning (sectorial scanning), beam focusing and so on. These sound beam manipulations help to achieve high reliability in flaw detection, improved accuracy in flaw characterization, high sensitivity and lower inspection time. These advantages make phased array an ideal candidate for in-service inspection of nuclear components. A mock-up with calibration reflectors in the form of side drilled holes (6 mm dia.) drilled at a distance of 425 mm from the top flange was fabricated. Two notches simulating the crack-type defects were introduced in the mock-up at a distance of 525 mm from the top flange surface. A linear phased array probe with a long aperture (5 MHz, 64 elements, 1 mm pitch) is used for this development. The phased array probe is positioned in the centre of the flange and focal laws are created to get multi-point focusing at a depth of 425 mm starting from ID of the vessel to the OD. This ensures that the entire weld area is examined from a single probe position. Another set of focal laws are created to focus the beam at a depth of 525 mm on ID and OD surface to look for crack-like defects. The scanning is carried out by moving the probe over the flange surface with these two sets of focal laws. C-scan images are collected during the scanning.

### Simulation Studies

Prior to the experimental work, ultrasonic simulation studies were carried out using CIVA NDE Simulation Package. These studies were aimed at computing appropriate set of focal laws for three purposes: (i) to examine the weld joint and the adjacent heat affected zone (HAZ) by using a focused sound beam, (ii) to examine the ID and OD surface of the RPV

shell to look for any crack like defects at a specific location (525 mm from top flange) and (iii) to examine the inside surface of RPV for any crack like defects at different depths from the top flange surface. Simulation studies involved the beam computation using various probe apertures and the computation of focal laws. Finally these focal laws are used in defect response module, the results of which are analyzed prior to taking up the experimental work.

### Sound Beam Computation

Fig. 2 shows the results of sound beam computation for examination of C1 weld joint.

For weld examination, the sound beam is focused at the depth of 425 mm, across the thickness of the RPV shell. This is achieved using Multi-point focusing. In this approach, the aperture is constant for all the focal laws, but the sequence in which the elements are fired changes as the focal point moves from the ID surface to the OD surface. The array of focal points is indicated in the extreme right image of the Fig. 2. For each focal point, one focal law is created. The focal laws are then applied shot after shot. The image in the middle represents the sound beam profile for one such shot, which is aimed at focusing the beam on ID surface. The image on the left is the combined result of all the shots put together. This image shows how the sound beam moves from ID to OD surface, shot after shot. In the above images, the intensity of sound beam is colour coded. Blue represents the maximum intensity and the pink represents the intensity slightly lower than the maximum. The marker corresponding to the depth of 425 mm from the top flange is also indicated in the image. The above image shows that a focused sound beam, as desired, is obtained at the weld location.

Fig. 3 shows the result of beam computation for the ultrasonic beam which is focused at a depth of 525 mm from the top flange surface. The objective

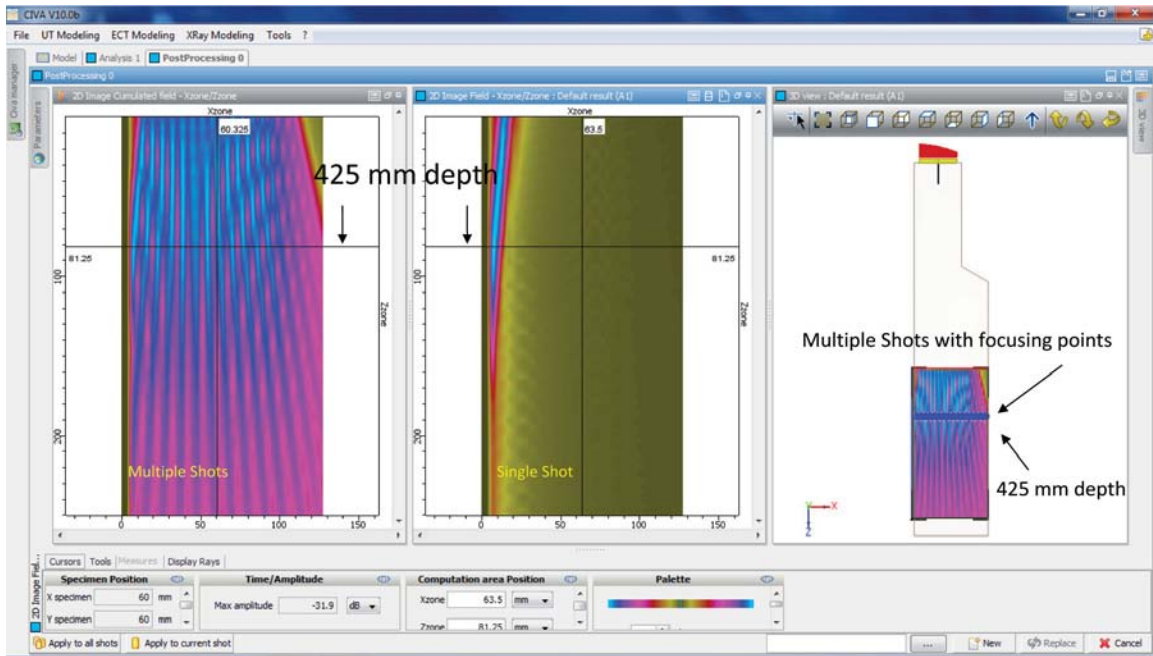


Fig. 2: Beam Computation for C1 weld examination

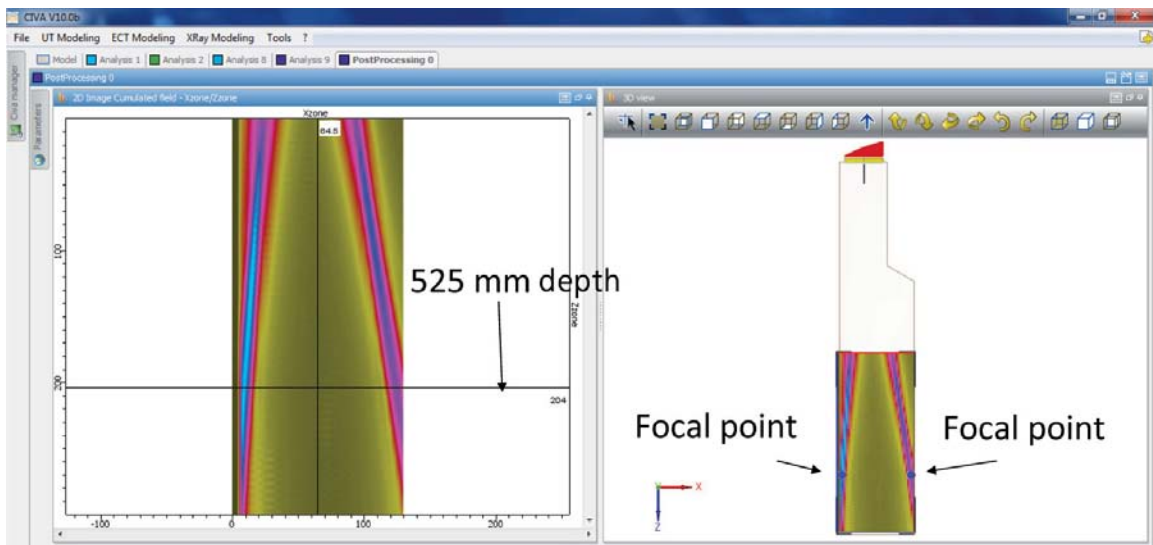


Fig. 3: Beam Computation for Crack detection in RPV shell

here is to find out any surface breaking flaw like cracks at ID and OD surface at this depth.

The image shows that the ultrasonic beam is focused at a depth of 525 mm on ID and OD surfaces. Two separate focal laws are used for this purpose. The focusing improves the sensitivity for detection of crack like defect.

Fig. 4. shows the result of beam computation for

the sound beam, which is focused on the ID surface at various depths. In this case the sequence in which the phased array crystals are fired remains same for all the focal laws. However the delays at which the elements are fired vary. The three images correspond to the sound beam profile when focused at a depth of 200 mm, 300 mm and 400 mm from top flange surface respectively. Once again, the images are colour coded. The maximum intensity (indicated by

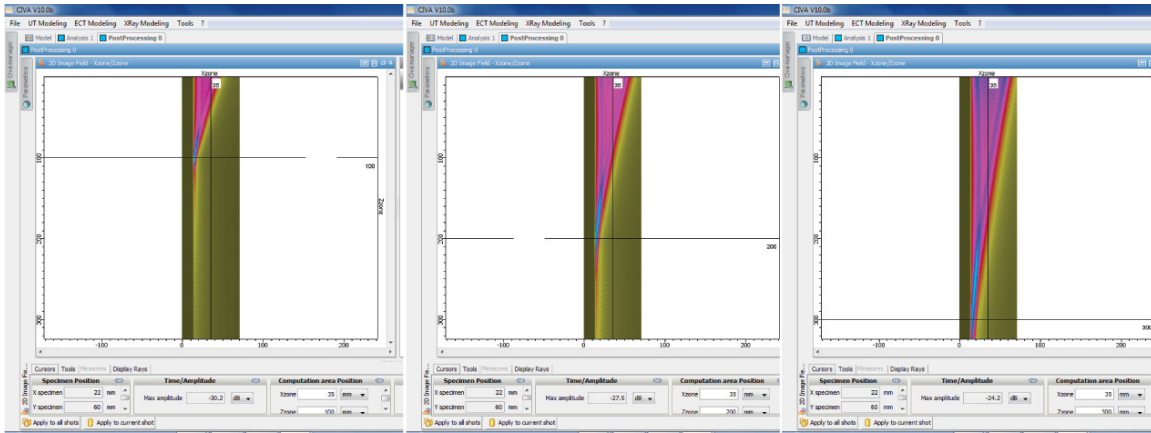


Fig. 4: Beam computation results for ID surface focusing at various depths

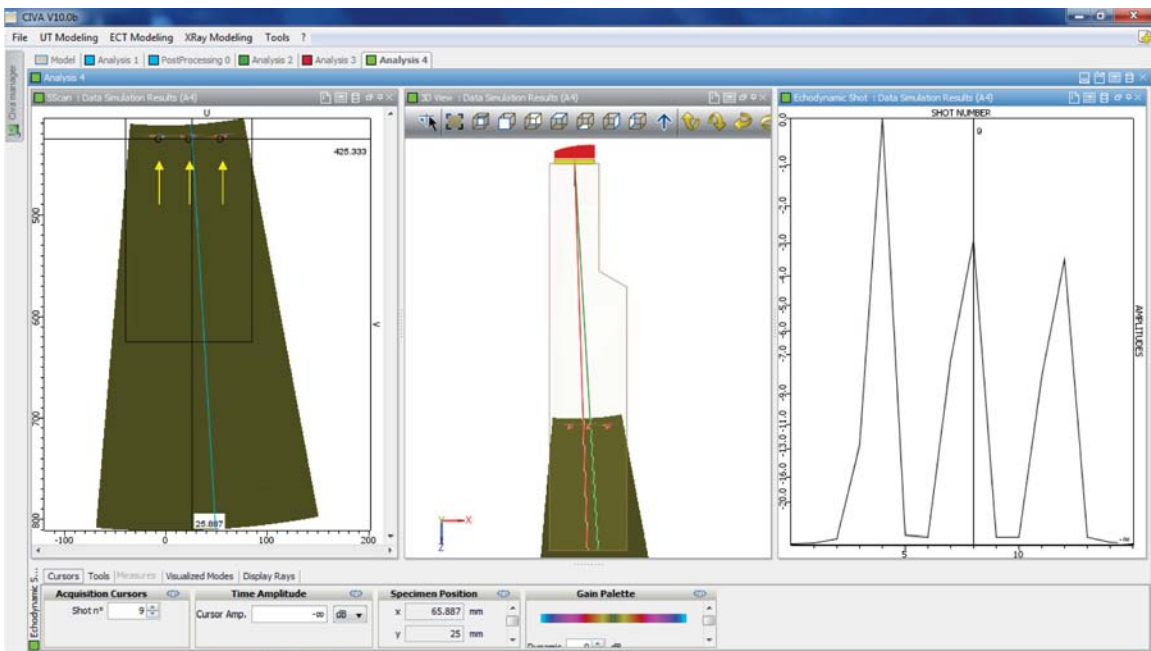


Fig. 5: Defect response during phased array examination for weld defects

blue colour) is seen on the ID surface at the respective depths.

**Defect Response Studies**

After the beam computation the effectiveness of the focal laws is assessed using the defect response module of CIVA. For this purpose, defects are introduced in the form of 6.3 mm dia. side drilled holes at a depth of 425 mm. Additionally ID and OD notches, 2.5 mm deep and 25 mm long, at ID and OD surfaces and fifteen notches of same dimensions on ID surface at varying depths starting

from 100 mm to 400 mm from the top flange surface are introduced. Fig. 5 shows the results of defect response analysis for the examination of weld joint. The above image shows that the three reference defects (side drilled hole) are picked up with good resolution (indicated by arrows in the leftmost image). The amplitude from the three defects also varies in a narrow range as indicated by the rightmost image. This indicates that the focal laws computed for weld examination using the beam computation module are effective for examination of C1 weld joint.

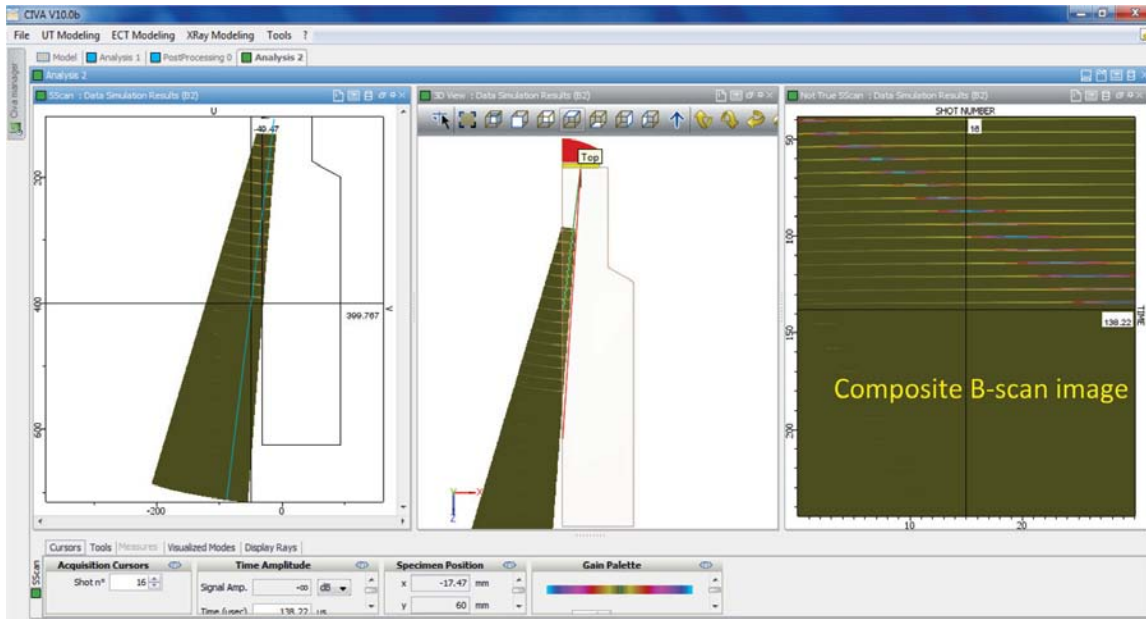


Fig. 6: Defect response for crack-like flaws on ID surface at various depths from the top flange

Fig. 6 shows the results of defect response analysis for notches placed at various depths on the ID surface. In order to detect these notches, the sound beam is focused at various depths using the multi-point focusing approach of phased array. In the present case, 15 notches (length 25 mm and depth 2.5 mm) are introduced at various depths starting from 100 mm up to a depth of 400 mm from the flange top surface. The results indicate that these flaws at various depths from the top flange surface are picked up with good amplitude.

The composite B-scan image for all shots (each shot corresponding to the focusing at a specific depth) is shown in the rightmost image. The image shows distinct signals from all the fifteen defects introduced at various depths. The amplitude from these defects varies in the range of 70% to 100%.

### Experimental Work

In order to develop the phased array technique, a mock-up piece was designed and fabricated. The mock-up piece is made of carbon steel. From ultrasonic point of view, both the carbon steel and low alloy steel, exhibit negligible sound attenuation

and similar sound velocity. Hence the use of carbon steel material instead of low alloy steel will not make any significant difference to the study. Another deviation in the mock-up is the fact that the mock-up does not contain any clad. During this study, the phased examination is being conducted from the top flange surface and not from the ID surface. Hence absence of clad on ID surface will not make any significant difference to the results. The mock-up fabricated for this development contains three side drilled holes at a depth of 425 mm from the scanning surface (top flange). These holes simulate the volumetric defects in the C1 weld joint. The mock-up piece also contains two notches on the side faces, simulating cracks on ID and OD surface of the pressure vessel. These notches are made at a depth of 525 mm from the scanning surface. A linear phased array probe of 5 MHz frequency, 64 elements, 1 mm pitch is used for the study. Additionally, scanning is also carried out using 4 MHz, 24 mm dia. conventional normal beam probe for the sake of comparison. The mock-up piece and the placement of phased array probe is shown in Fig. 7.



Fig. 7: C1 weld mock-up

The mock-up of C1 pressure vessel weld is examined using linear phased array probe and M2M make 64 x 256 Multi 2000 phased array system. In order to perform the scan, the phased array probe is first

positioned on the top flange as shown in Fig. 7. It is then moved over the top flange for the entire width of the mock-up. During the scanning a C-scan image is collected. For conventional ultrasonic testing, the probe is placed on the top flange at the locations at which the side drilled holes and the notches could be picked up. The probe is moved over the flange from ID surface to the OD surface. During this movement B-scan image is collected.

**Results and Analysis**

Fig. 8 shows the B-scan image for the holes using the conventional probe and Fig. 9 shows the B-scan image using the phased array probe.

These images reveal how phased array is effective in getting a very good resolution due to the focusing effect. While the three side drilled holes are not seen separately in the B-scan image using conventional probe, they are well defined using phased array. Apart from the resolution the focusing of sound beam also improves sensitivity, which

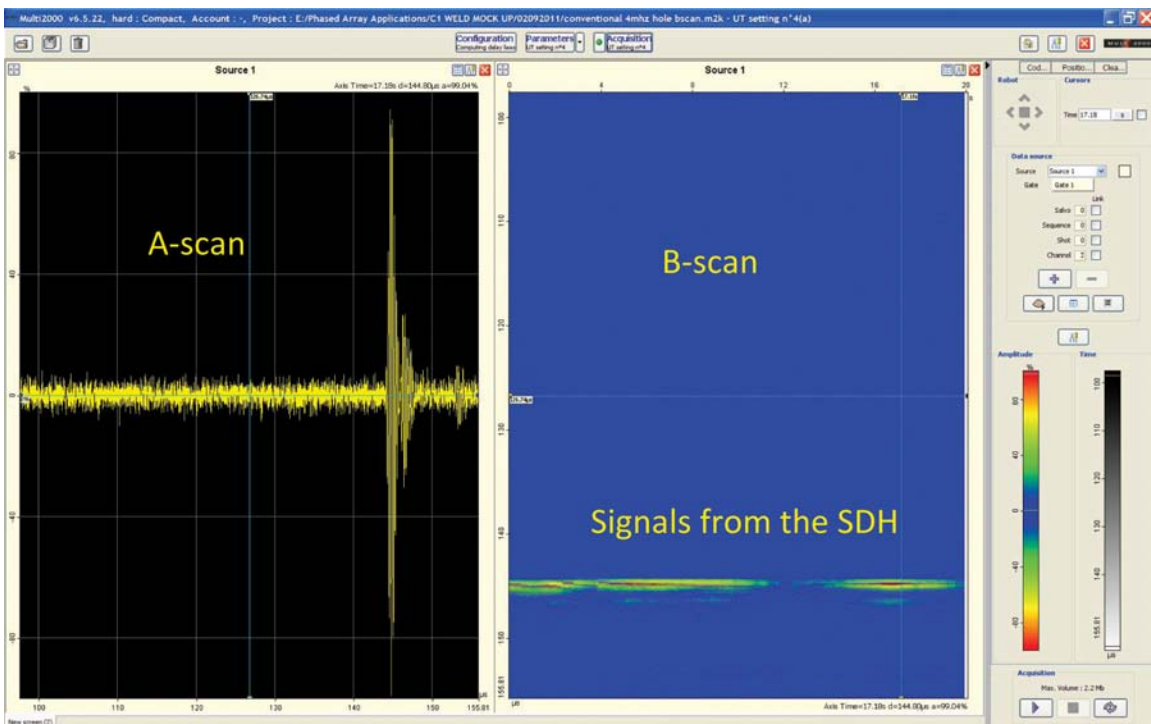


Fig. 8: B-scan image for holes using conventional normal beam probe



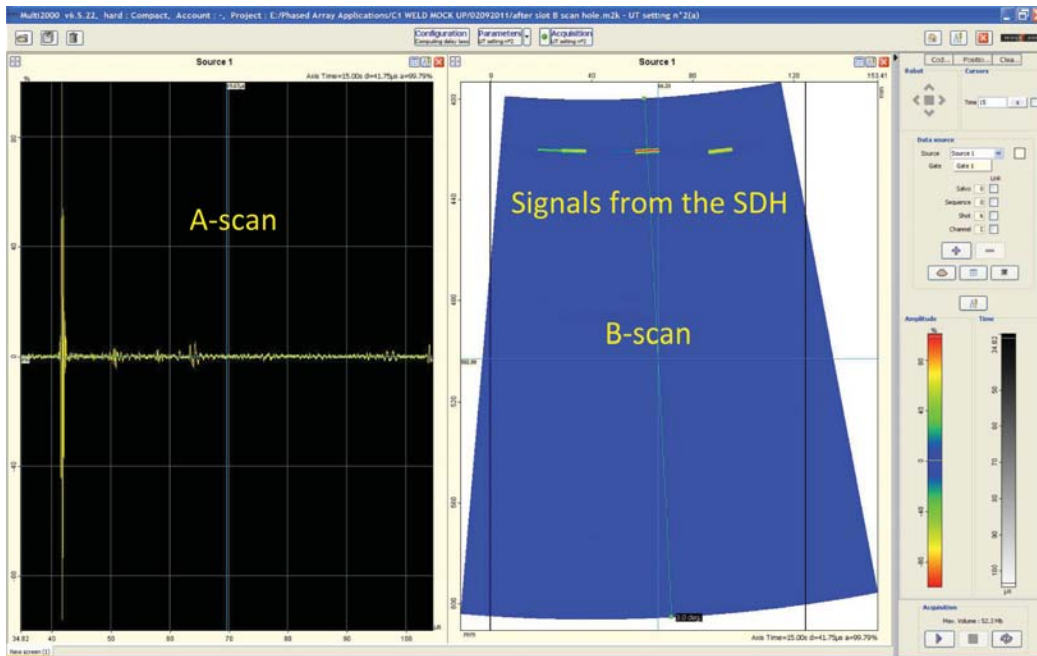


Fig. 9: B-scan image for holes using phased array probe

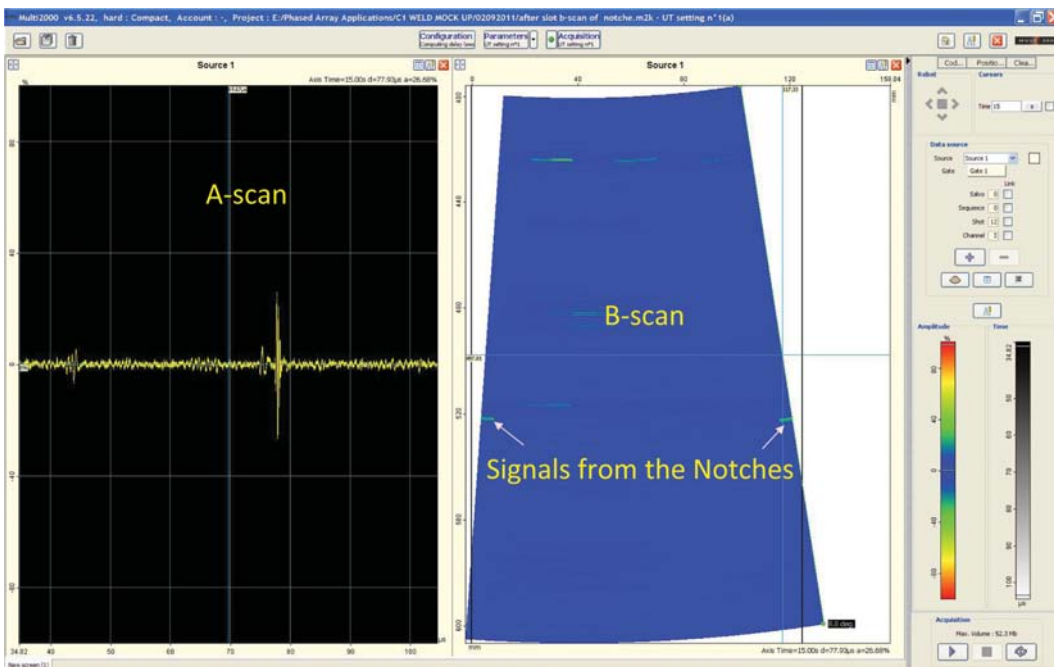


Fig. 10: B-scan image for notches using phased array probe

means one can detect smaller defects using phased array. The A-scans for the conventional probe and the phased array probe shows that the noise level is much lower using phased array as compared to conventional probe.

Fig. 10 shows the B-scan image for the notches at the depth of 525 mm using phased array probe. The notches could not be picked up using conventional probe even after increasing the amplifier gain. As a result there is no image for notches to

compare between the conventional ultrasonic method and the phased array method.

This image shows that notches on ID and OD are also well detected using phased array probe.

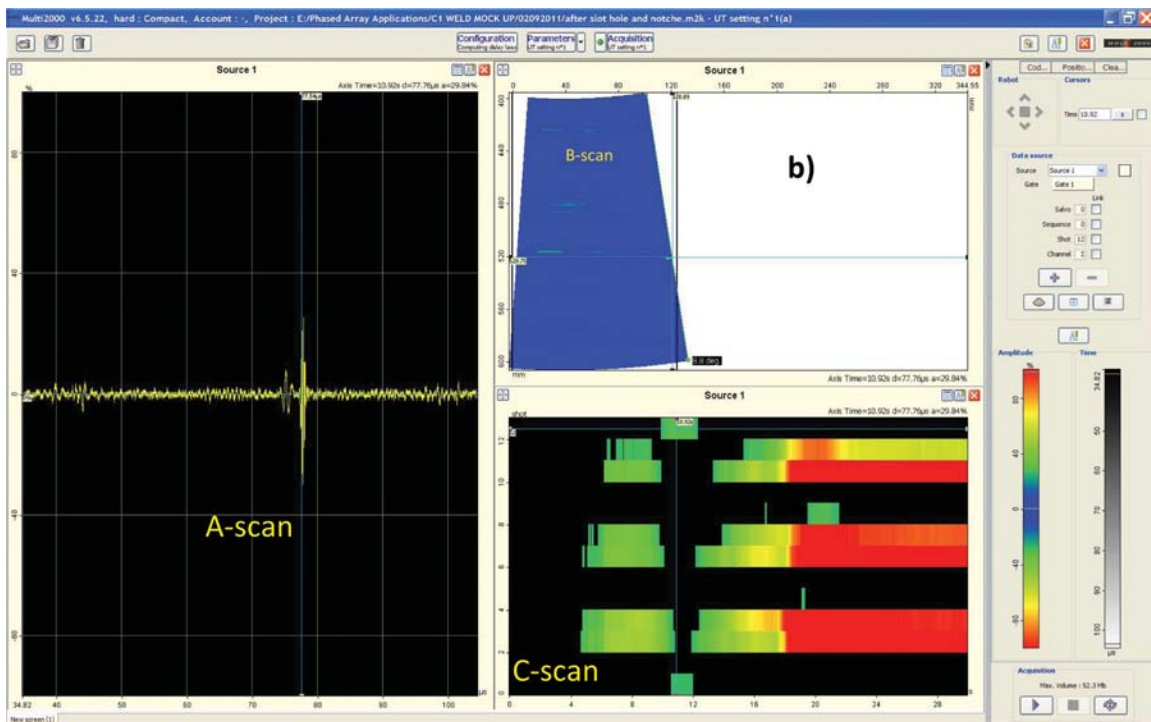
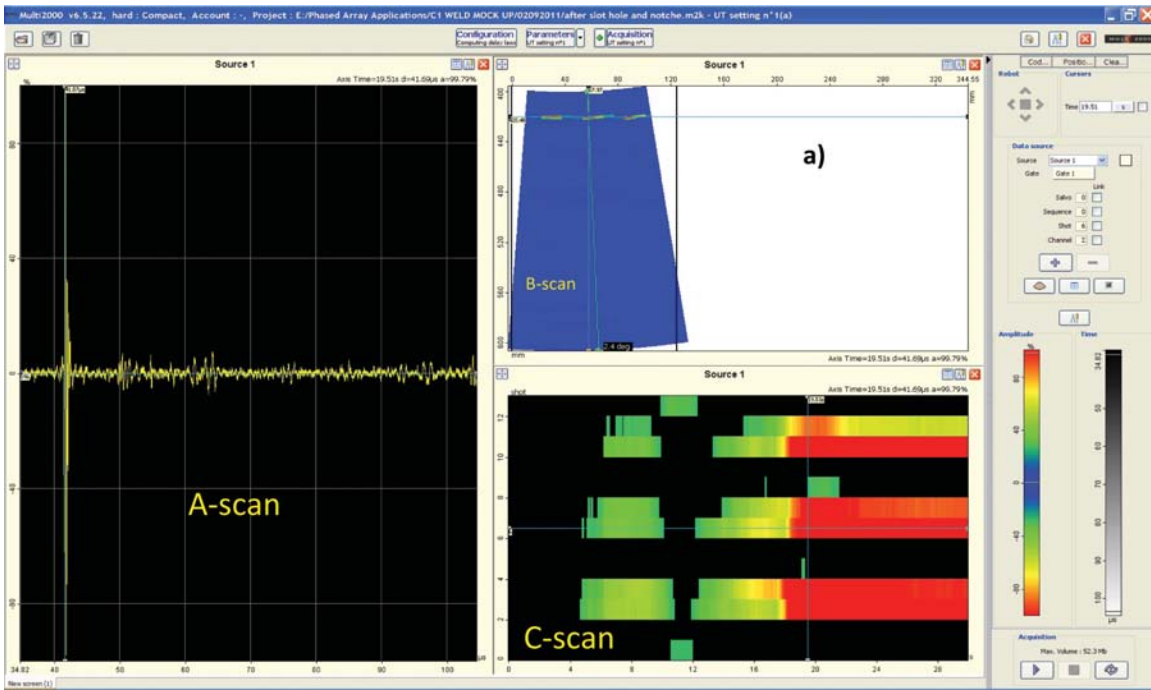


Fig. 11: Composite A, B and C-scan image during phased array examination of pressure vessel weld mock-up: a) At side drilled hole location, b) Notch location

Although the signal amplitude for notches is lower as compared to that from side drilled holes, the signal to noise ratio is quite high. This ensures that cracks of the order of these dimensions in the circumferential radial plane will be detected using phased array.

Figs. 11 a and b show the C-scan image acquired during scanning using phased array probe. The B-scan image and the A-scan corresponding to notch location are also put alongside.

These two figures show the composite A, B and C-scans at two locations during scanning, (a) corresponding to the location of side drilled hole and (b) corresponding to the location of notches.

The C-scan shows that the side drilled holes simulating the volumetric flaws in the C1 weld joint and the notches corresponding to the crack-like defects at depths even farther than the weld joint are well detected. The B-scan image at hole location shows three distinct signals corresponding to three holes. The A-scan shows high amplitude of the reflected signal. The results indicate that the focusing of the sound beam at this depth has been effective. The B-scan at notch location shows distinct signals from two notches, one at ID and the other at OD. The amplitude from these notches as indicated by the A-scan (although lower than the side drilled holes) is well above the noise level. This ensures that the focal laws applied during phased array examination have been effective.

## Conclusions

The phased array inspection of pressure vessel weld of BWR offers several benefits. First and foremost is the fact that it will ensure 100% volumetric examination of pressure vessel weld. The beam steering achieved by phased array focal laws helps in 100% examination of the weld joint from a single probe location. The presence of bolting penetrations in the top flange surface offers no hindrance to achieve effective inspection using phased array. This has been demonstrated by experiments on the mock-up, which not only simulates the presence of volumetric flaws in weld joint at the required depth, but also the obstruction due to the bolting penetrations. Another advantage offered by phased array examination is the detection of crack like defects in the circumferential-radial plane on ID and OD surface, even at a depth of 525 mm. The use of multi-point focusing approach along the vessel ID by phased array will detect these cracks starting from ID surface at various depths from the top flange surface.

## Acknowledgements

The authors wish to acknowledge the contributions of Shri Santosh Salunkhe and Shri Harvendra Singh from QAD, BARC for carrying out the experimental work for development of phased array technique for RPV weld inspection. The authors would like to express their gratitude towards Shri S. Anantharaman, Head, QAD and Dr. G.J. Prasad, Director, NFG for their encouragement and support.

# Fuel Handling System Training Simulator for 540 MWe PHWR

Vinaya Kumar

Fuel Handling Control Section  
Electronics & Instrumentation Group

## Abstract

Fuel handling system in Pressurised Heavy Water Reactors has always generated a lot of interest and attention because of the need for on-power refuelling. Execution of large number of steps in a predefined sequential order and the interlocks based on continuous monitoring of various signals characterize on-power refueling operation on a selected reactor channel. The large number of intricate and complex operations involved during execution of these sequences needs thorough understanding, in order to skillfully handle the faults or malfunctions. Proper operation by trained crew can prevent occurrences of off-normal and emergency situations. Simulator training and re-training are uniquely capable of dealing with many of the main recurring problems in the development, qualification and evaluation of the plant operators.

## Introduction

BARC & NPCIL had entered into an MoU in January 2006 for the design and development of fuel handling system (FHS) training simulator for TAPS-3&4. This development was taken up at Fuel Handling Control Section (FHCS), BARC. Phase-1 of the simulator was commissioned in February 2009, Phase-2 in March 2011 and now Phase-3 is commissioned in December 2011 at NTC, Tarapur. The system is being utilized to provide in-depth training and qualification for Control Engineer (Fuel Handling) and Trainee Control Engineers.

## System Architecture

FHS Training Simulator is configured around network of 15 PC nodes and a PC as system gateway node (SGN). Client-Server model of communication consists of a Server handling data transfers among 14 Client nodes. Seven nodes for north side and seven nodes for south side implement refueling process of the two sides on a reactor channel. [Fig. 1]

The nodes are arranged spatially in such a way that each side trainee operator has access to six PCs: two operator interface systems (FM-OIS, FT-OIS),

two soft panels (FM,FT manual/ vertical panels), one auxiliary panels/ hydraulic display station (HDS) and one 3-D mimics to provide in-depth knowledge of the refueling operations through mechanical and process mimics on 42 inch plasma display panel (PDP).

Instructor is provided with three PCs: north dynamic simulator, south dynamic simulator and data server. D<sub>2</sub>O and oil hydraulics circuits are implemented in dynamic simulator so as to perform 'emergency operating procedures (EOPs)' totaling to about 50 nos. Un-editable form of the hydraulic circuits is available at HDS to trainees for guidance during training for EOPs.

## Software Design

Full duplex network is established using a 1Gbps Ethernet Switch, Windows Socket as the basic building block for communication and TCP/IP for data transfer. Software of all the nodes is developed in Visual C++ using 'Visual Studio.NET 2005 & 2010' and runs under WindowsXP/ Windows 7 operating system.

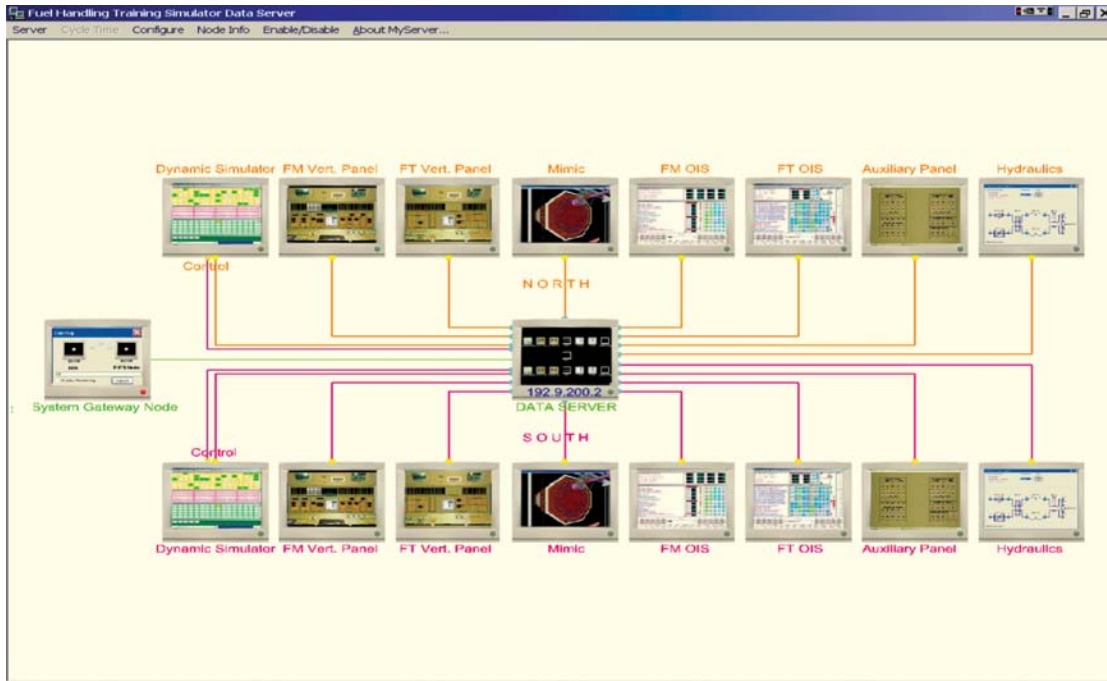


Fig. 1: PHWR Fuel Handling System Training Simulator Deployment Diagram (TAPS-3&4)

Design pattern approaches in software design have been widely used with a view to capture software design know-how and make it reusable. Builder pattern and composite pattern are used in soft console development. Singleton pattern, proxy pattern, composite pattern, subject-observer pattern and strategy pattern are used in dynamic simulator development.

For instance, subject-observer pattern has been chosen for interaction of fuelling machine rams while it is moving with various other components. All rams and fuelling machine magazine act as a subject and have complete state information of their observers sorted spatially. Only subjects have the prerogative to change the states of the observers during its movements. Hence this pattern defines clean and standard interaction of classes for system logical simulation.

Because the two side fuelling machines work in tandem during refuelling operation, one from north side and the other from south side, proxy pattern has been used for exchange of data from other side

during refuelling. Thus these two patterns have been extensively made use of while designing dynamic simulator application.

### Nodes with Instructor

Instructor keeps track of the training simulator system status through Server node and introduces various normal and abnormal scenarios during training sessions through Dynamic Simulator node. Server facia displays connectivity status of all the nodes and the connecting links are displayed using appropriate colours. For each node, it shows the IP address, number of packets transferred/ received and the comparative data transfer speed visualization by showing moving balls on the data link between nodes.

These features of server help in system diagnosis. In order to maintain the integrity of the state of the application running on a Client node, a node dependency protocol is implemented for connection & disconnection of the nodes with the Server. The Client node will be forcefully disconnected by the

Server if the user fails to disconnect a dependent node during shutdown or tries to connect a node in, out of order sequence during system startup.

Execution of control system software and simulation of fuel handling system is carried out in dynamic simulator node. This node is the heart of the training simulator system as it executes all algorithms of control system and models of mechanical systems and hydraulic circuits with provision to introduce variety of malfunctions during training sessions. Various parameters (speed, force, extreme positions, delay timers, etc.) associated with these models can be viewed and altered by Instructor by using appropriate dialog boxes. Instructor can initialize the fuel handling system status at the start of the training session through initialization dialog box.

The control system software consists of system software written in C++ and the application software written in process control language (PCL). The application software implements fuel handling operations logic, checks all safety interlocks and issues commands to operate the field devices which can be seen on the mimics. Cycle time of 50 msec. is maintained to provide real time features as in the control systems at nuclear power plants (NPPs).

### **Operator Interface System (OIS)**

Operator Interface Systems for fueling machine and fuel transfer (FM-OIS and FT-OIS) for each of the two sides, are identical in all respect with the ones available in reactor control room. OIS enables issue of commands to carry out all the refueling sequences in auto mode and the actuation of all the field devices in computer manual mode. It provides all the necessary displays and messages about refueling status through various windows on the screen. The messages are disk logged which enables analysis of the trainee's performance

### **Control Room Soft Consoles**

Large size monitors (30 inch) having very high

resolution (2560 x1600) is used for soft panels. The panels can be moved up/down, right/left and zoom in/out in order to focus at a particular area of operation. However, a position named 'Operating or Home View' is created and provided with 'Home' hot key of the keyboard which gathers the maximum pane of the operating console. It is now observed that the soft panels require only horizontal scrolling at times for operating the pumps on the sloping part of the panels and these operations are rare. Now the soft panels have become very close to replica hard panels.

The panels contain variety of actuating and indicating buttons, DPMs, alarm enunciators and PID controllers. Using design patterns in software design, each component such as button, lamp or controller is developed as separate class in object oriented concept using OpenGL. As OpenGL supports depth dimension along with the length and breadth dimensions, the soft consoles implement the true angular dimensions of control panels thereby giving the perception of 3-D console. Each button of the console responds to mouse click event irrespective of camera position.

Soft consoles read the information about console components through Microsoft Excel files. Automation, formerly called "OLE Automation," technology has been used. It allows the functionality like Microsoft Excel into the applications. Each console component exposes a set of interfaces through which all communication to the component is handled.

In order to provide very realistic display of various instruments on the soft panel, original pictures have been used for all the console components. Using these image files and applying the Trilinear Mipmapping technique, the original texture has been applied to the soft console components. The name plates of the sub panels are described using texture mapping for various titles and sub-titles. [Fig. 2]



Fig. 2: FM Manual Panel (North) – Soft Console

### Auxiliary Soft Consoles

Auxiliary panels include: NFM local panel, FM service area door panel, sealing door panel, shielding door panel, vault door panel, FT room door panel, roll on shield panel and spent fuel transfer control panel. These are small panels consisting of indicator lamps and actuating pushbuttons. Any one of the auxiliary panels can be selected one at a time for operation.

### Hydraulics

D<sub>2</sub>O and oil hydraulics logical modeling is implemented and integrated with mechanical system models in dynamic simulator node in such a way that both application modules can be independently

developed and integrated in a standard and clean interface manner. Hydraulic system circuit design is based on standard design patterns so that it can be easily adaptable for various components as well as systems. This involved designing basic structural pattern of classes, interface between various hydraulic objects, hydraulic circuits, user interface dialog boxes, and interface with the existing models of dynamic simulator and implementation of EOPs through hydraulic circuits. [Fig. 3a & b]

### 3-D Mimics

Various popular options were considered for development of 3-D mimics. These consisted: Libraries (OpenGL, Direct-X and Java 3-D), Packages (Maya, Render Man, Idea and 3-D Studio Max etc.) and Editors (VRML – Virtual Reality Modeling Language). It was decided to use OpenGL embedded in VC++ programming language. On-line 3-D mimics have been implemented for reactor channel refueling, fuel transfer operations and spent fuel transfer operations.

Complete fuel handling operations, right from bundles loaded from loading trough to new fuel magazine (NFM), bundle transferred from NFM to transfer magazine (TM), bundles exchanged inside

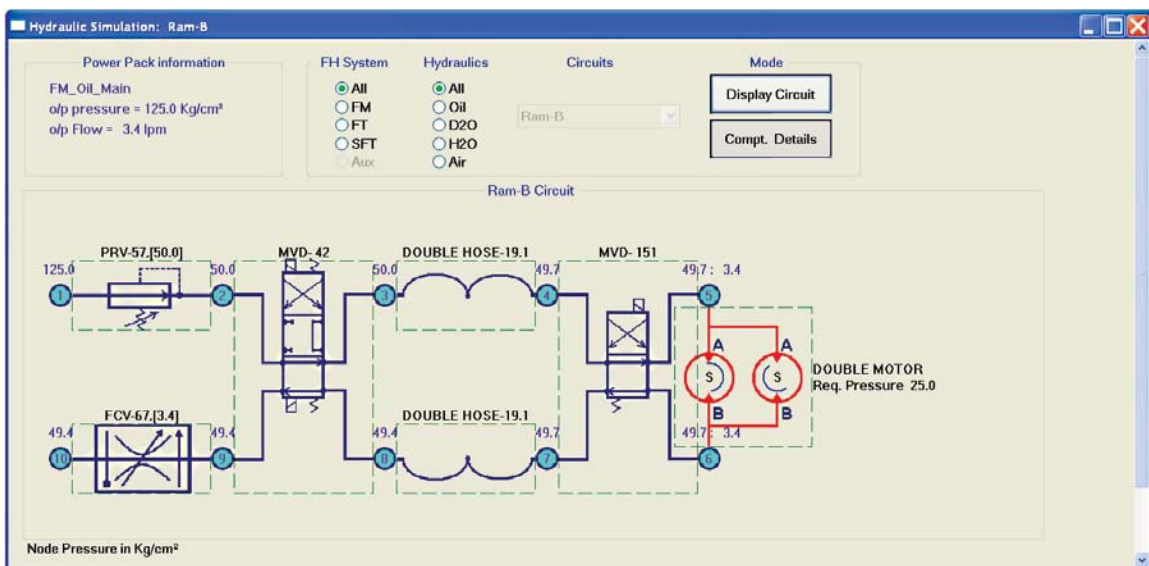


Fig. 3a: Hydraulic circuit "Ram-B" runs with faulty condition in Motors.

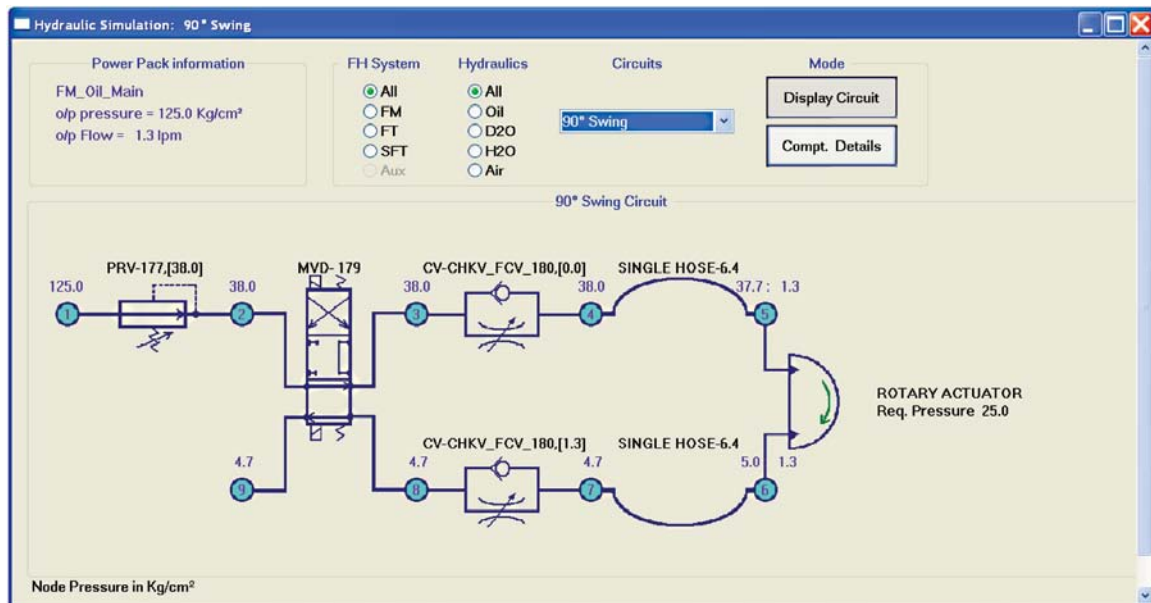


Fig. 3b: Hydraulic circuit "90° Swing" in "Display circuit mode"

the channel including plug operations, spent fuel received from fuelling machine to TM to shuttle transfer station (STS) and bundles transferred from STS to Shuttle Receiving Tube (SRT) via shuttle transfer tube (STT) are all shown in online mimics during execution of refueling sequences. Occlusion culling technique has been used to render components, which is to be finally seen on the scene based on camera position.

Various Component internals like springs and 'O' rings are drawn using blending technique and Stencil test. Billboard technique is used for surfaces, which have uniform pattern along with various axial angles. Billboard is a technique that adjusts an object's orientation so that it faces camera. NURBS (Non Uniform Rational B-Spline) have been used to show compression in sealing disk of seal plug. Particle Systems using Textures are used for showing water sprays in the mimics. Various advanced techniques like Transparency, dynamic ordering of Z-Buffer, Accumulation Buffer and culling methods have been used to depict and render this 3-D mimic.

Mimics use varied color-coding scheme, symbols and modes to add worth in training and learning.

The components shown in mimics can be depicted in different states namely: red rectangle state, yellow rectangle state, blue rectangle state and green rectangle state, to show different situations. Stop-sign and Retracted-component symbol are used appropriately. Mimics can be shown in two different modes i.e. wire frame mode and solid mode (opaque as well as transparent). Each of these modes can be rendered as 2-D, 3-D or cut view of 3-D.

Wire frame mode depicts how the rendering of the component is done using lines and a viewer can see the internals of components without being obstructed by the external surfaces. Solid mode depicts actual surface of the component. 2-D view focuses on the internal mechanism of interaction and is especially useful to provide details of plug operations in reactor channel. Cut view gives advantage of both views, i.e. on one side it gives the actual and true appearance of the component and on the other side it focuses on the interaction mechanism. [Fig. 4]

Special effects like: water flow through reactor channel and through STT, horizontal and vertical spray of water for cooling of hot fuel bundles during



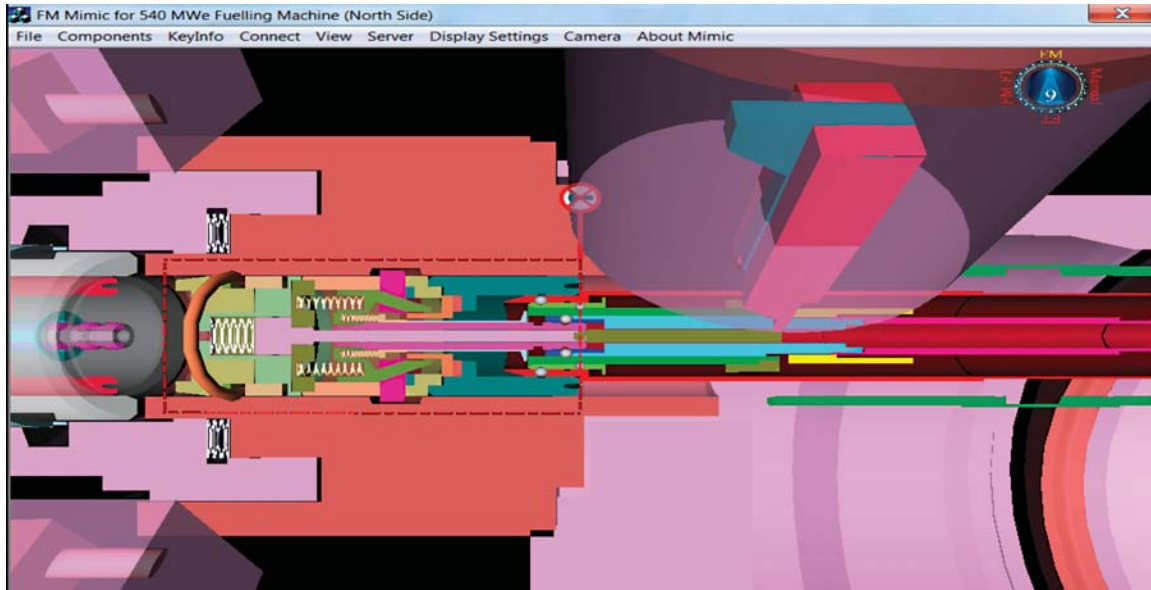


Fig. 4: Mimic of Plug Operation (Plug Moving With Ram Assembly)

dry transfer operation when hardware timer timeout condition occurs in fuel transfer (FT) system etc. have been implemented in 3-D mimics. Texture mapping using blending is used for water flow effect and particle system algorithms are written to show water droplets falling during water spray. Link list is used to generate and delete water particles during run time. OpenGL embedded in VC++ has been found suitable for implementing these special effects. Though many higher level 3-D packages claim to have these special effects but none of them claim to run it under real time in online mode. Recently, some packages like Virtool (virtual tool) have become available which claim to provide effects in real time and it is yet to be verified.

### Camera Positions

For viewing the mimics, camera can be placed by the user in three different automatic tracking modes associated with fuelling machine, fuel transfer system and spent fuel transfer system. The camera can also be operated in the manual mode. At each automatic tracking mode there are distinct positions which the camera traces to depending upon the location of the action taking place. These distinct camera positions have been tabulated and described in design

manuals. New positions of camera can be easily created as desired. In case more than one action is taking place at any time, the camera will place itself based on the priority of the action as preset in the implementation. Distinct positions of camera are labeled mathematically as an integer number (post fixed by an alphabet if camera takes different state for a position while monitoring a long travelled component) and this can be seen inside the camera tracking symbol.

Manual mode of camera is chosen when user wants to navigate inside the mimic on its own using the keys assigned for navigation. In this mode user can move up/down, left/right, zoom in/out and rotate clockwise/anticlockwise. During manual mode operation, user may save camera position of interest as bookmarks and name the bookmark as per the view available e.g. if the user bookmarks the zoomed position of the seal plug, he can name it as the 'close-up of seal plug'. Next time the user can directly view any of the bookmarked positions. Once user is done with the manual mode he can switch to the last automatic mode selected and camera will automatically place itself intelligently at the point of action.

Online mimics of refueling sequences can be saved as .avi (audio video) format as video file for demonstration by Instructor as offline mimics using a standalone PC. These .avi formats can be compressed as .divx or .mp4 format using tools (like Super) for archival storage.

### Software Protection

All the nodes of training simulator communicate to external world only via SGN, which prevents unauthorized entry of malicious software. SGN has protection installed against all the malwares (virus & worms) with latest virus definitions. SGN gives pathway to load all the simulator system software in various nodes. All other nodes execute complex real time software needing all the resources of the node, interact with each other to maintain process cycle time of 50 msec and therefore would not be burdened with extra processing associated with software protection. Therefore, the access medium (CD, DVD, USB device) of these 15 nodes are disabled to avoid unauthorized/ unintended corruption.

### Software Upgrades

Version control has been implemented in the training simulator software of each node to keep track of incrementally different versions of software. Version number is the number that identifies the specific release and revision of software and consists of several different values: major, minor, build/release and an optional quantifier. Since, Visual C++ doesn't have a feature to automatically increment the version number resource information of the software being developed after each build or released, a version controller has been developed for the purpose.

Version control feature is very useful as new versions are released since the development work has followed phased approach. Progressively, features are incorporated in the training simulator for providing training in handling more EOPs. Nuclear

Training Center (NTC) maintains a list of EOPs which are updated as per the operating experience.

### Benefits

The project of training simulator development has offered many challenging opportunities and promoted team work among the developers group. It has been breeding ground of innovative ideas for software development associated with simulation, operator interface, networking and 3-D mimics. These are now being gainfully applied in the development of fuel handling control systems of AHWR and PFBR at FHCS.

### Concluding Remark

PC network based FHS Training Simulator for TAPS-3&4 commissioned at Nuclear Training Center, Tarapur offers cost effective and flexible system to very effectively meet the requirements of Fuel Handling System operator training and licensing requirements.

### Acknowledgements

The simulator developers' team consists of Shri Anup Suryawanshi, Shri Vikas Diwan, Shri Ramesh B. Adelli, Shri Dinesh K. Maurya and Shri Nikhil Saxena of FHCS. Significant contributions are also from Shri B. Ganaraja, Shri K.P. Sarkar, Smt. Geetha S. Kumar and Smt. Nalini Singh Patel of FHCS. At NTC, Tarapur, Shri Anil Seth (Training Superintendent), Shri P. Mohanti and Shri S.S. Ghevade provided valuable support in commissioning of the system at site. At NPCIL, Mumbai, Shri A.K. Purandare and Smt. Libiba Behal played key role in co-ordination. Shri Umesh Chandra (Sr ED-Sefty & KM) facilitated the MoU and provided support.

The author thanks Shri R.K. Patil, Associate Director (C) and Shri G.P. Srivastava, Director, Electronics & Instrumentation Group, BARC for their keen interest and support for this work.

# ANUPAM-Adhya Supercomputer

K. Rajesh, K. Bhatt, D.D. Sonvane, K. Vaibhav,  
V. Duggal, U. Karnani, N. Chandorkar, K.R. Koli,  
R.S. Mundada and A.G. Apte  
Computer Division

## Abstract

Modern day scientific research increasingly relies on high speed computers in some stage or other. This is true of BARC too, where a large number of scientists and engineers are engaged in research in advanced fields of science and engineering. Computer Division, BARC has developed the ANUPAM series of supercomputers to cater to this ever-increasing demand for computing power. The latest in the series of ANUPAM systems is the ANUPAM-Adhya supercomputer, developed in 2010-11 with a sustained performance of 47 Teraflops. This system is released to users and is being used extensively. This article describes the new supercomputer, its architecture, subsystems and some applications that run on the system.

## Introduction

BARC is a premiere research organization working on the development, demonstration and deployment of technologies related to nuclear reactors, nuclear fuel cycle, isotopes and radiation applications. It carries out inter-disciplinary and multi-disciplinary R&D activities covering a wide range of disciplines in physical sciences, chemical sciences, biological sciences and engineering. Expertise at BARC covers the entire spectrum of science and technology. More than 4000 scientists and engineers working on various advanced R&D at BARC are extensively using computers for meeting their requirements of supercomputing, general scientific computing, scientific visualization, information processing and information exchange.

Computer Division, BARC has a mandate of providing centralized computing facilities for the scientists and engineers of BARC, a significant number of which work in fields that require access to high speed computers. The complex problems that these users attempt to tackle are such that they cannot be solved on conventional desktops or servers in a reasonable amount of time. The ANUPAM Supercomputer project, undertaken by Computer Division has been fulfilling this ever-increasing

demand for number crunching power for the last two decades.

High Performance Computing is a branch of computer science that deals with the design, development and use of computer systems that have performances much exceeding those in normal everyday use. These machines are characterized by large processor performances, large memory sizes and large storages. Supercomputers are used for solving compute intensive problems in areas such as nuclear physics, weather forecasting, climate research, molecular dynamics, computational fluid dynamics, structural analysis and other problems commonly called Grand Challenge problems. The philosophy behind supercomputing is to divide such big tasks across multiple processors available in a supercomputer and get the job done in parallel and thus in a reasonable amount of time. Many of the scientific applications fall under HPC category and require supercomputers to solve the problems efficiently.

## ANUPAM Series of Supercomputers

Computer Division, BARC has started development of supercomputers under the ANUPAM project in

1991 and till date, has developed more than 20 different computer systems. All ANUPAM systems have employed parallel processing as the underlying philosophy and MIMD (Multiple Instruction Multiple Data) as the core architecture. BARC, being a multidisciplinary research organization, has a large pool of Scientists and Engineers, working in various aspects of Nuclear Science and Technology and thus are involved in doing diverse nature of computations. To cater to the computational needs of this diverse set of users, the ANUPAM supercomputers have been developed as general-purpose parallel computers. To keep the gestation period short, the parallel computers were built with commercially available off-the-shelf components, with our major contribution being in the areas of system integration, system engineering, system software development, application software development, fine tuning of the system and support to a diverse set of users. The graph in Fig. 1 shows the road-map of ANUPAM Series of Supercomputers, with the year of inception on X-axis and the performance of the system on Y-axis.

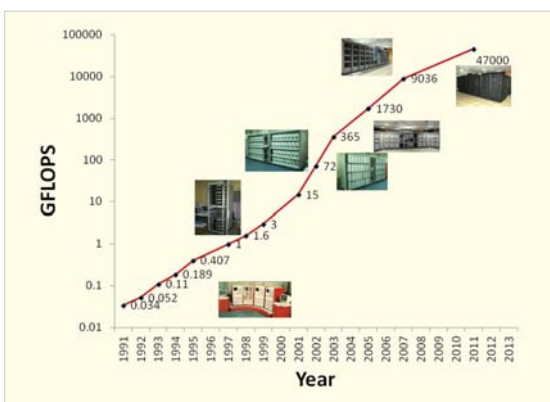


Fig. 1: ANUPAM Performance over the years

The series started with a small 4 processor system in 1991 with a sustained performance of 34 MFLOPS. Keeping in mind the ever increasing demands from the users, new systems have been built regularly with increasing computational power. The latest in the series of supercomputers is the 4608 core ANUPAM-Adhya system developed in 2010-11, with a sustained performance of 47

TeraFLOPS on the standard High Performance Linpack (HPL) benchmark. The system is in production mode and released to users. The detailed architecture of ANUPAM-Adhya system is described in the following sections. Fig. 2 is a photograph of ANUPAM-Adhya.



Fig. 2: ANUPAM-Adhya

### ANUPAM-Adhya Architecture

The ANUPAM-Adhya supercomputer consists of the following subsystems:

#### Compute subsystem

The Compute Subsystem is the computational workhorse of the system, the place where user jobs are run and their problems get solved. This subsystem also determines the overall performance of the supercomputer. The compute subsystem of ANUPAM-Adhya is made up of 576 compute nodes, with each node having two Quad Core 3.0GHz processors and 32GB 800 MHz DDR2 FBDIMM memory. Thus, there are a total of 4608 processing cores, each with a peak performance of 12 GFLOPS. Scientific Linux 5.5 is used as the operating system along with OpenMPI, MVAPICH and MVAPICH2 libraries providing parallel environment. Since the number of computing cores in ANUPAM-Adhya is finite, the system should ensure that each user gets her fair share of the available resources. This is done by a resource management system which maintains

queues of user jobs and schedules jobs in the system using a fair share policy. Different queues have been implemented to cater to the needs of a variety of job types such as sequential jobs, long jobs, short jobs and so on.

### ***Infiniband Interconnection Network***

ANUPAM-Adhya consists of two independent interconnection networks – a primary network using Infiniband and a secondary network using Gigabit Ethernet. The Infiniband network is used for inter-process communication by jobs and Network File System I/O. The Gigabit Ethernet network is used for installation and management tasks.

Anupam-Adhya uses 4x DDR Infiniband network as a primary interconnect. 4x DDR Infiniband provides low latency (4 microseconds) and high bandwidth (20 Gbps) network for inter-process communication. Ideally, in order to connect 576 nodes in an Infiniband network, we need a network switch that has 576 ports in it. Since the largest infiniband switch commercially available at the time was of 288 ports only, the required 576 node network had to be realized using a multistage network using many switches.

In order to achieve best performance figures from an infiniband network, it is necessary to build them with 100% non-blocking factor, also called fully non-blocking. To construct a 576 port fully non-blocking network using 288 port switches, we need 6 numbers of 288 port switches and 1152 infiniband cables. Managing these many switches and cables was always going to be difficult; hence other less complex switch configurations were investigated. It was found out using experiments that even a 50% non-blocking network resulted only in insignificant drops in job performance but with much less switch and cabling complexities. Hence it was decided to build a 50% non-blocking network using one 288 port core switch and 36 numbers of 24 port edge switches. Fig. 3 shows the diagram of the network.

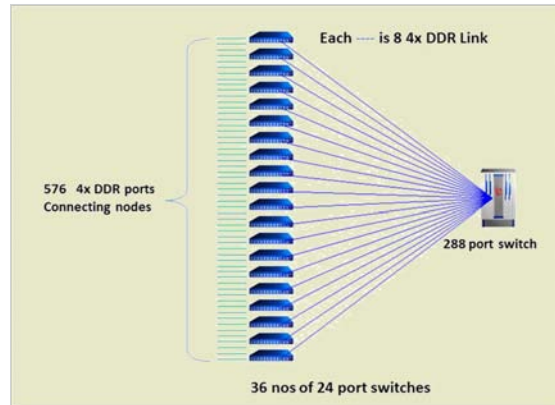


Fig. 3: ANUPAM-Adhya Infiniband network

Switching fabric of Infiniband network is managed by a subnet manager running inside the central switch. It sweeps the network regularly and generates its topology to determine the optimal route between the nodes. Since system has a 50% non-blocking network, the subnet manager uses a “top-down” routing algorithm to determine the routing tables instead of default balanced algorithm used for full non-blocking network.

### ***Storage Subsystem***

Storage is one of the critical components of a high performance computing system, which affects the usability of the system by the users. Traditional storage subsystems such as direct access storage and network access storage suffer from the lack of scalability and manageability when used for building large storage subsystem of the order of hundreds of terabytes. Storage Area Network (SAN) based systems separate the actual storage part from the servers and thus provide better scalability and reliability. Moreover, SAN based storage systems provide advanced features such as access control, volume management, snapshots (point-in-time copies), synchronous and asynchronous replication are critical to the design of a full-fledged storage system and play an important role in data security and disaster recovery.

ANUPAM-Adhya has a 100 Terabyte SAN based storage subsystem that is based on iSCSI Storage

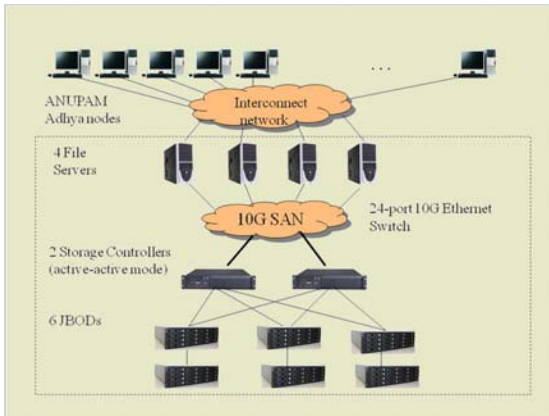


Fig. 4: ANUPAM-Adhya Storage subsystem

protocol. Fig. 4 shows the architectural diagram of the storage. The design of the system is modular, which means upgradation and enhancement in storage is easy. The 100 TB SAN storage system is housed in a 42U rack along with ANUPAM-Adhya that consists of the following components:

**Storage Targets:** These are two storage controllers connected in active-active mode for high availability and six SAS disk arrays (JBODs) each hosting 16 1-Terabyte SAS Disks.

**File Servers / Initiators:** Four file servers act as a frontend to the SAN storage. The compute nodes requests data to the file servers over NFS, the file servers in turn access the data from Storage Targets using iSCSI protocol over 10G Ethernet network.

**Storage Network:** A 24-port 10 G Ethernet switch provides the connectivity between the storage targets and the file servers/initiators.

**Heat Removal Sub-system**

ANUPAM-Adhya has 4608 computing cores, which are distributed in 576 servers and these servers are distributed across 12 standard 42U, 19 inch racks. Each rack dissipates 22KW of heat under full load and this heat needs to be removed efficiently to keep the system temperature under control. At 22 KW heat load per rack, each rack needs to be

supplied with 72000 litres of cold air per minute (2540 cfm) to remove the heat with a Delta T of 15 degrees Celsius. Traditional heat removal methods employed in computer centres such as in BARC are not able to handle this kind of dense heat loads. To solve the problem of heat removal, an advanced chilled water based heat removal system was deployed. Water is a far better coolant than air because of its high specific heat (four times that of air) and high density (800 times that of air). Only 40 litres of water per minute are needed for a 22KW rack with 8 degrees C delta T. The 12 server racks were arranged in two rows, each row containing 6 server racks and 7 air-water heat exchangers. Cold air is blown through the server racks, where the heat dissipated by the servers is transferred to the air. The heat absorbed by air is immediately transferred to chilled de-mineralized water by the air-water heat exchangers. The requirement of 2500 cfm of air for cooling is fulfilled by large size blowers that circulate air from the server racks to the air-water heat exchangers. De-mineralized water is used as a primary coolant and this water is cooled by chilled water from the central AC plant by means of water-water heat exchangers. The reason behind using demineralized water in the primary circuit is that it is non-conductive, ultra-pure, contains no particulate matter and hence poses less risk to electronics in case of leakage. And, the purpose behind using two coolant circuits is to limit the flooding of water up to the amount of water in the

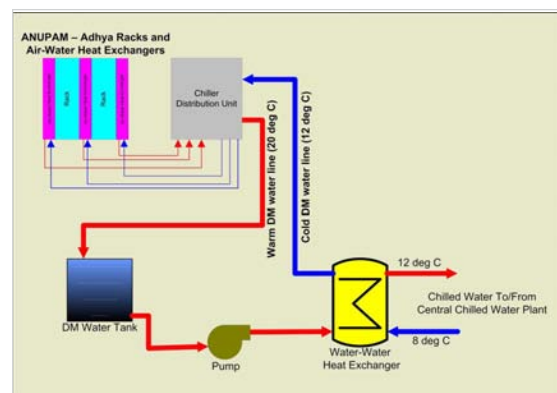


Fig. 5: Heat Removal Subsystem

primary circuit in case of failure in water pipe. The schematic of the heat removal sub system is shown Fig. 5.

### ***Environment Monitoring and Protection System***

The ANUPAM-Adhya supercomputer is arranged in 12 racks with each rack consisting of densely packed servers. Since this electronic hardware is sensitive to high temperature, it is necessary to continuously monitor the heat removal system for any variation in temperature. For this purpose, an integrated central environment monitoring system is developed to monitor environmental parameters, such as temperature and humidity of the system continuously. The monitoring system frequently reads environmental parameters from large number of sensors placed in the system racks and stores these values in a database. It also analyzes this data to detect abnormal changes and alerts the operator. The operator can track the current environment around the system using a web interface.

Since the ANUPAM-Adhya supercomputer dissipates about 240 KW of heat in a totally enclosed rack space, a failure of supply of chilled water can cause a temperature increase of tens of degrees with a space of a few minutes. Unless attended to immediately, this can have a catastrophic effect on the electronic components of the system. In order to cater to such circumstances, a protection system is put in place with three independent protection schemes.

- In case of break in water supply due to failure of a water pump, the air-water heat exchangers are configured to send traps. These traps are caught by listening software that immediately triggers a safe shutdown of the system.
- The BIOS of all the server machines are configured in "STAY OFF" mode so that whenever the power resumes after a failure, the power of server machines remain off and

can be switched on once the cooling system is restarted after the power failure.

- In every server machine the processor temperature is monitored using the IPMI tools. If the temperature crosses the limit of 45 degrees, the server is automatically shutdown.

### **System Software for ANUPAM-Adhya**

A large system such as ANUPAM-Adhya needs a wide gamut of software to keep it running and available to users. The software environment of the system is made up of components that are a mix of free and open source software along with several in-house developed tools and utilities. Scientific Linux 5.5 is the operating system that runs on all nodes of the system. The program development and runtime environment comprises MPI implementations such as MVAPICH and OpenMPI and numerical libraries such as BLAS.

Several in-house monitoring and management tools such as Anunetra (monitoring), AnuInstall (Rapid deployment), Anupam Accounting system (User Job accounting), AnuSakshi (Hardware Life Cycle management) and Load Sharing and Queuing system, which were used in earlier supercomputers are also used in the ANUPAM-Adhya. Some of the newer software development efforts are listed below

#### ***LDAPSync***

Earlier ANUPAM systems made use of synchronized local files for storing user authentication information. Because of limitations of this approach, this technique was abandoned in favour of centralized LDAP based authentication in ANUPAM-Adhya. But the centralized authentication scheme was found to have scalability issues, especially during the boot process. During boot up, hundreds of nodes tried to communicate with the LDAP server simultaneously, thereby exhausting the resources of the LDAP server. To overcome these issues LDAP sync utility is developed, which regularly

synchronizes the user information from central LDAP server to local files. If the central server is down then the information is not refreshed but still the old information can be used for authentication. A random sleep is used to randomize the connection time of nodes to LDAP server, to provide load balancing and avoid resource scarcity and connection denial at server. Currently this system is being successfully used in ANUPAM-Adhya supercomputer.

### ***Use of Virtualized Service nodes***

Any ANUPAM system has several nodes that run critical services to keep the system running. Some of these critical services are the authentication service, resource management service, installation service, management and monitoring services and so on. Even though, it was possible to run multiple services on a single machine as in smaller systems, the approach was abandoned in larger machines in order to eliminate dependencies between services and failure of multiple services when a shared host failed. In earlier large ANUPAM systems, each service ran on a separate dedicated node. Nowadays with nodes having multiple cpu cores, running each service on a dedicated machine seemed a waste of computing power. Therefore, in ANUPAM-Adhya a new approach has been used for hosting these services. Each service now runs within a dedicated virtual machine. Multiple virtual machines are hosted within a single physical machine. This solves the problem of wastage of resources and also does not compromise service isolation. Since these virtual machine images are backed up, it is easy to re-deploy them in another host in case of hardware failures

### **User Applications**

The ANUPAM-Adhya supercomputer is being used by scientists and engineers of BARC in solving computationally intensive problems in diverse fields ranging from physics, chemistry and engineering.

The applications that run on ANUPAM-Adhya are a mix of in-house developed, open source and commercially purchased applications. The results obtained have enabled the scientists to publish their research work in prestigious international journals in physics and chemistry. Some of the work done is listed below:

- Study of new materials and their properties under extreme conditions
- Exploring interplay of structural, magnetic, optical and transport properties of a wide range of novel and emerging material systems
- Study of nano-materials and nano-catalysts
- Micro-mechanical analysis of PHT piping in reactors
- MACE telescope simulation studies
- Designing suitable materials for reversible hydrogen storage, fuel cell and water splitting
- Molecular Dynamics (MD) simulations of Bio-macromolecules in Explicit Solvent
- Study of Electric response properties of carbon nanostructures
- Study of properties of artificially synthesized elements
- Design of new drugs to combat radiation damage
- Study of radiation damage in materials
- Structural, electronic and magnetic properties of Bimetallic Nanowires
- Design and screening of ligand/solvent system for metal ion separation and isotope separation
- Applications in nuclear waste management

The following pictures depict the outputs of some of the applications that run on ANUPAM-Adhya.

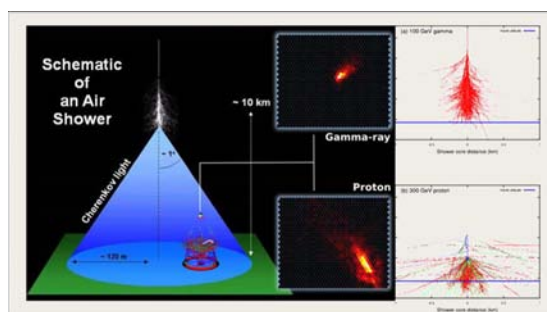


Fig. 6: MACE Telescope Simulations



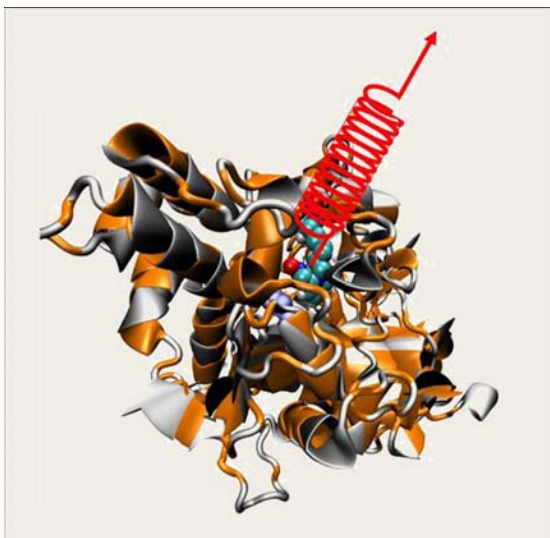


Fig. 7: Unbinding of drug molecule bound to the active-site of protein molecule

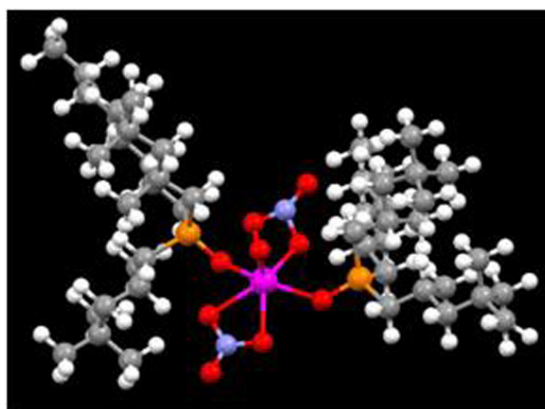


Fig. 9: Ligand/Solvent system for metal ion separation and isotope separation

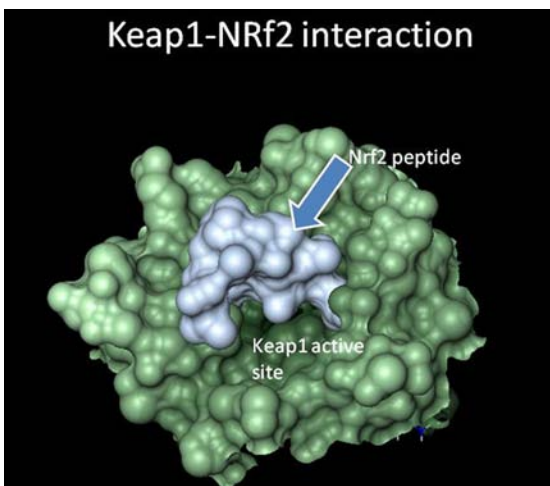


Fig. 8: Design of new drugs

### Acknowledgements

Building and commissioning a large supercomputer such as ANUPAM-Adhya requires team effort from a large number of people. We gratefully acknowledge the efforts of the operations and administrative staff of Computer Division for full support during the work. The help of the erstwhile Infrastructure Projects Division (now part of TSD) in setting up of the heat removal system and the Technical Services Division for electrical support is also acknowledged. We thank Desalination Division for supplying the demineralized water for ANUPAM-Adhya's heat removal system. We also thank the users of the system for keeping the system fully utilized and their inputs for this article.

# Biosensors for Environmental and Clinical Monitoring

Jitendra Kumar and S. F. D'Souza

Nuclear Agriculture and Biotechnology Division

## Abstract

Biosensors are analytical devices composed of a recognition element of biological origin and a physico-chemical transducer. Immobilization plays a major role in developing the biosensor by integrating both the above components. In this article, studies carried out at BARC on immobilization of biological elements and their association with transducers for the development of biosensors for environmental and clinical monitoring, are reviewed. Biosensors for methyl parathion pesticide, catechol, glucose, urea, cholesterol and dopamine are being studied

## Concept of Biosensor

A biosensor is a compact analytical device, incorporating a biological or biologically derived sensing element, either closely connected to, or integrated within a transducer system. The principle of detection is the specific binding of the analyte of interest to the complementary biorecognition element immobilized on a suitable support matrix (Fig. 1). The specific interaction results in a change

in one or more physico-chemical properties (viz. pH change, electron transfer, mass changes, heat transfer, uptake or release of gases or specific ions) which can be detected and measured by the transducer. The usual aim is to produce an electronic signal, which is proportional to the concentration of a specific analyte or group of analytes, to which the biosensing element binds<sup>1-2</sup>.

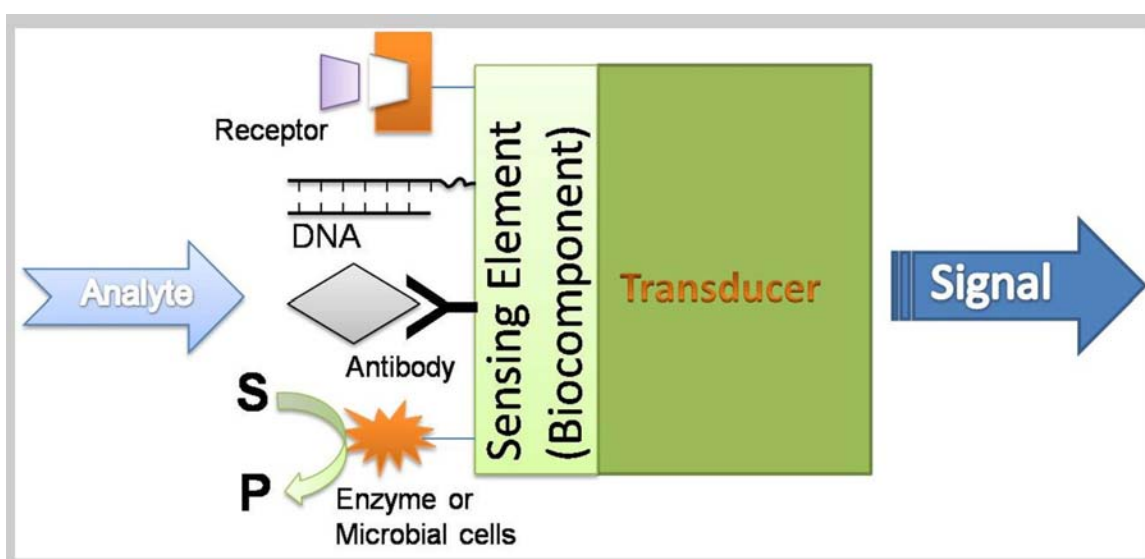


Fig.1: Principle of biosensors

Biosensors can be classified according to bio-recognition system. The biological elements used in biosensor technology are the enzymes, antibody/antigens and nucleic acids/complementary sequences. In addition, microorganisms, animal or plant whole cells and tissue slices, can also be incorporated in the biosensing system. Depending on the method of signal transduction, biosensors can also be divided into different groups: electrochemical (amperometric, potentiometric or conductometric), optical, thermometric and piezoelectric. Biosensors offer many advantages over conventional analytical techniques. The selectivity of the biological sensing element offers an opportunity for the development of highly specific devices for real-time analysis in complex mixtures, without the need for extensive sample pre-treatment or large sample volumes. The function of a biosensor will depend on the biochemical specificity of the biologically active material. Biosensors also promise highly sensitive, rapid, reproducible and simple-to-operate analytical tools. Biomolecules have poor stability in solutions hence it is necessary to stabilize them by immobilization. Thus immobilization plays a key role in developing stable biocomponent for integration with transducers<sup>1-2</sup>.

This review summarizes some of our studies related to immobilization of biological molecules on different supports using suitable techniques for the development of biosensors for environmental and clinical monitoring.

### **Biosensor for Environmental Monitoring**

Towards monitoring of different environmental pollutants, our laboratory has been working on the development of biosensors for pesticides and phenolic compounds. Methyl parathion pesticide is extensively used in the field of agriculture despite its high toxicity and contributes a major share in terms of restricted use in India. Among the various biosensors for methyl parathion detection, major systems are based on acetylcholinesterase (AChE)

and organophosphorus hydrolase (OPH) enzymes. AChE biosensor is based on enzyme inhibition mechanism, hence it requires longer incubation time and also has poor specificity because of interference from carbamate pesticide and metals. OPH catalyzes hydrolysis of methyl parathion pesticide into detectable product *p*-nitrophenol (PNP) and generates two protons as a result of the cleavage of the P-O bond. Products that are chromophoric and/or electroactive can be detected by colorimetric and electrochemical methods, and are exploited to develop biosensors for detection of methyl parathion pesticide. The analyte can be determined, as the rate of product formation is directly proportional to the concentration of the analyte. As the OPH is a periplasmic enzyme, whole cells can be immobilized directly on the matrix and integrated with transducers for biosensor development. In our laboratory different types of microbial biocomponents (from disposable to reusable) were developed by immobilizing microbial cells on different supports and associated with different transducers (optical and electrochemical) for simultaneous analysis of single to multiple samples. An optical microbial biosensor was developed in which disposable biocomponent was prepared by immobilizing whole cells of *Flavobacterium sp.* on glass fibre filter paper disc and associated with an optical fibre transducer for the detection of methyl parathion<sup>3</sup>. In the second study, *opd* gene, which codes for OPH enzyme, was cloned to make recombinant *E.coli* with high periplasmic expression of enzyme. Recombinant *E.coli* cells were immobilized on screen-printed carbon electrode (SPCE) for preparing the biocomponent and an electrochemical microbial biosensor was developed based on cyclic voltammetry for the detection of methyl parathion. In this study, biocomponent was reusable and biosensor required low volume of sample<sup>4</sup>. In our third study, an optical biosensor was developed for detecting a large number of samples in a single platform in a short period of time. For this, a soil bacterium, *Sphingomonas sp.*

JK1 was isolated and identified which hydrolyzes methyl parathion. Microbial cells were then immobilized onto the surface of the wells of microplate (96 wells) and used as a reusable biocomponent, providing a convenient system for simultaneous analysis of multiple numbers of samples. In another experiment, *Sphingomonas sp.* JK1 was also immobilized on the inner epidermis of onion bulb scale as a natural support and directly placed in the wells of microplate and associated with the optical transducer for monitoring of methyl parathion pesticide <sup>6</sup>.

Phenolic compounds include a large variety of analytes having significance in health care and environmental pollution monitoring. Phenolics constitute a large group of pollutants, which originate from a variety of industrial processes such as manufacture of plastic, paper, dyes, drugs and pesticides. Catechol is one such phenolic derivative which is readily absorbed by the gastrointestinal tract, causing vasoconstriction, renal tube degeneration, decrease in liver function, cancers, and neurodegenerative diseases. Tyrosinase is a polyphenol oxidase enzyme that catalyzes the oxidation of phenolic compounds via hydroxylation with molecular oxygen to catechols and subsequent dehydrogenation to *o*-quinones which can be reduced at low potentials. Hence this enzyme was employed for the development of a biosensor for low potential detection of phenols and catechol in foods, pharmaceuticals, and clinical and environmental samples. In one study, tyrosinase enzyme was entrapped in agarose–guar gum composite matrix and an electrochemical biosensor was developed for catechol<sup>7</sup>. In another study, tyrosinase was also entrapped on oxidized porous silicon and a conductivity-based biosensor was developed for quantitative estimation of catechol <sup>8</sup>.

### Biosensor for Clinical Monitoring

Enzymes are well-known as biological sensing materials in the development of biosensors due to

their specificity and play a key role in clinical diagnosis. Enzymes like glucose oxidase (GOD), urease, choline oxidase (ChOx) and tyrosinase etc., were immobilized on suitable supports for better stability and reusability and associated with transducers for biosensor monitoring of clinical metabolites such as glucose, urea, cholesterol and dopamine etc.

Detection of glucose has been the most studied analyte in diabetic patients. Most of the glucose biosensors are based on the glucose oxidation catalyzed by GOD. Immobilized GOD converts glucose into gluconolactone with the consumption of oxygen. Amperometric response was monitored, by measuring the depletion of oxygen from sample using oxygen-sensitive dissolved oxygen (DO) electrode. A method was optimized to prepare a synthetic polyvinyl alcohol (PVA) membrane using high and low degree of polymerization of PVA, acetone, benzoic acid and cross-linking by UV treatment and GOD was immobilized and integrated with the DO probe for biosensor application<sup>9</sup>. GOD was also immobilized on inner epidermal membrane of the onion bulb scales as a natural support and applied for biosensor application for detection of glucose in association with DO probe <sup>10</sup>.

Urea estimation is of utmost importance in monitoring kidney functions and associated disorders. Determination of blood urea nitrogen is an important routine test widely used in clinical laboratories. Urease is one of the key enzymes which can be utilized for developing urea biosensor. The catalytic action of urease over substrate urea liberates ammonium ion, which can be detected by ammonium ion selective electrode as transducer. In our studies, urease enzyme was entrapped in PVA and polyacrylamide (PAA) composite polymer membrane prepared on the cheesecloth support by gamma-irradiation induced free radical polymerization and urea biosensor was developed. The performance of the biosensor was monitored using a flow-through cell in conjugation with the

ammonium selective electrode and ammonium produced as a result of enzymatic reaction was monitored potentiometrically<sup>11</sup>. Whole cells of *Brevibacterium ammoniagenes*, as a source of urease, were also immobilized in polystyrene sulphonate–polyaniline (PSS–PANI) conducting polymer on a Pt twin wire electrode, by potentiostatic electropolymerization and the change in resistivity of the sensor was used for calibration of the urea biosensor<sup>12</sup>.

Cholesterol is an important lipid found in cells and membrane of all animal tissues. High cholesterol accumulation in the blood serum is strongly correlated with diseases such as coronary heart disease, arteriosclerosis, brain thrombosis, lipid metabolism dysfunction and cerebral infarction (stroke). Decrease in the level of cholesterol in blood causes hyperthyroidism, anemia, malabsorption and wasting Syndrome. Cholesterol oxidase (ChOx) enzyme can be used for the development of a biosensor for the determination of cholesterol. Immobilization of ChOx onto the electrode surface is a critical step. A method was developed for immobilization of positively charged ChOx and the negatively charged multi walled carbon nanotubes (MWCNTs) on graphite electrode surface using layer-by-layer technique. The modified electrodes showed electrocatalytic activity towards reduction of oxygen which was associated with cyclic voltammetry and electrochemical impedance spectroscopy for the determination of cholesterol<sup>13</sup>.

Dopamine plays an important role in the function of central nervous, renal, hormonal and cardiovascular systems. It is of great clinical importance to measure the dopamine level in extracellular fluid to monitor neurotransmission processes and diagnose Parkinson's disease. We have used tyrosinase for the development of dopamine biosensor. Tyrosinase was extracted from a plant source *Amorphophallus campanulatus* and immobilized in a novel composite of two biopolymers: agarose and guar gum. The composite

matrix-containing enzyme forms a self-adhering layer on the active surface of glassy carbon electrode, making it a selective and sensitive biosensor. Modified electrode was associated with electrochemical analyzer to determine dopamine by direct reduction of biocatalytically liberated quinone<sup>14</sup>. In another study, tyrosinase was also immobilized on glutaraldehyde activated eggshell membrane for the development of an electrochemical biosensor for dopamine detection<sup>15</sup>.

## Conclusion

Microbial OPH and tyrosinase enzymes were used for the development of biosensors for the environmental monitoring of methyl parathion and catechol. Biosensors were also developed using immobilized GOD, urease, ChOx and tyrosinase for monitoring of clinical metabolites glucose, urea, cholesterol and dopamine respectively, for clinical analysis.

## References

1. D'Souza, S. F. Immobilization and Stabilization of Biomaterials for Biosensor Applications. *Applied Biochemistry and Biotechnology - Part A Enzyme Engineering and Biotechnology* 96 (2001): 225-38.
2. D'Souza, S. F. Microbial Biosensors. *Biosensors and Bioelectronics* 16 (2001): 337-53.
3. Kumar, J., Jha, S. K., and D'Souza, S. F. Optical Microbial Biosensor for Detection of Methyl Parathion Pesticide using *Flavobacterium Sp.* Whole Cells Adsorbed on Glass Fiber Filters as Disposable Biocomponent. *Biosensors and Bioelectronics* 21 (2006): 2100-05.
4. Kumar, J., and D'Souza, S. F. "Microbial Biosensor for Detection of Methyl Parathion using Screen Printed Carbon Electrode and Cyclic Voltammetry." *Biosensors and Bioelectronics* 26 (2011): 4289-93.

5. Kumar, J., and D'Souza, S. F. An Optical Microbial Biosensor for Detection of Methyl Parathion using *Sphingomonas Sp.* Immobilized on Microplate as a Reusable Biocomponent. *Biosensors and Bioelectronics* 26 (2010): 1292-96.
6. Kumar, J., and D'Souza, S. F. Immobilization of Microbial Cells on Inner Epidermis of Onion Bulb Scale for Biosensor Application. *Biosensors and Bioelectronics* 26 (2011): 4399-404.
7. Tembe, S., Inamdar, S., Haram, S., Karve, M., and D'Souza, S. F. Electrochemical Biosensor for Catechol using Agarose-Guar Gum Entrapped Tyrosinase. *Journal of Biotechnology* 128 (2007): 80-85.
8. Tembe, S., Chaudhari, P. S., Bhoraskar S. V., D'Souza S. F., and Karve M. S. Conductivity-Based Catechol Sensor Using Tyrosinase Immobilized in Porous Silicon. *IEEE Sensors Journal* 8 (2008): 1593-97.
9. Kumar, J., and D'Souza, S. F. Preparation of PVA Membrane for Immobilization of GOD for Glucose Biosensor. *Talanta* 75 (2008): 183-88.
10. Kumar, J., and D'Souza, S. F. Inner Epidermis of Onion Bulb Scale: As Natural Support for Immobilization of Glucose Oxidase and its Application in Dissolved Oxygen Based Biosensor. *Biosensors and Bioelectronics* 24 (2009): 1792-95.
11. Jha, S.K., Topkar, A. and D'Souza, S.F. Development of Potentiometric Urea Biosensor Based on Urease Immobilized in PVA-PAA Composite Matrix for Estimation of Blood Urea Nitrogen (BUN). *Journal of Biochemical and Biophysical Methods* 70 (2008): 1145-50.
12. Jha, S.K., Kanungo, M., Nath, A. and D'Souza, S.F. Entrapment of Live Microbial Cells in Electropolymerized Polyaniline and their use as Urea Biosensor. *Biosensors and Bioelectronics* 24 (2009): 2637-42.
13. Manjunatha, R., Nagaraju, D.H., Suresh, G.S., Melo, J.S., D'Souza, S.F. and Venkatesha, T.V. Direct Electrochemistry of Cholesterol Oxidase on MWCNTs. *Journal of Electroanalytical Chemistry* 651 (2011): 24-29.
14. Tembe, S., Karve, M., Inamdar, S., Haram, S., Melo, J., and D'Souza, S. F. Development of Electrochemical Biosensor Based on Tyrosinase Immobilized in Composite Biopolymeric Film. *Analytical Biochemistry* 349 (2006): 72-77.
15. Tembe, S., Kubal, B.S., Karve, M. and D'Souza, S.F. Glutaraldehyde Activated Eggshell Membrane for Immobilization of Tyrosinase from *Amorphophallus Campanulatus*: Application in Construction of Electrochemical Biosensor for Dopamine. *Analytica Chimica Acta* 612 (2008): 212-17.

# Groundwater Contamination Problems in Rural India: Detection and Remediation at the Household Level

S.C. Chaurasia, A.C. Sahayam, G. Venkateswarlu, S.M. Dhavile, S. Thangavel and L. Rastogi

National Centre for Compositional Characterization of Materials (CCCM), Hyderabad

and

T. Mukherjee

Chemistry Group

## Abstract

Contamination of ground water with Arsenic, Iron, Manganese and Bacteria is causing concern in India particularly in North Eastern States and West Bengal. Analysis of the water sample in these areas indicates contamination well beyond acceptable limits set by the World Health Organization (WHO). Researchers have been working on solutions to this problem in terms of simple methods of detection of the contamination and remedial measures at the household level. This article brings out results of water sample analysis for West Bengal and North Eastern States. Simple detection technique for ground water contamination and its remedial measures are also covered.

## Introduction

Groundwater problems such as pH, iron, manganese, arsenic, bacteria and fluoride of North Eastern States and West Bengal have been detected and remediated at household level. Water is treated with  $\text{KMnO}_4$  followed by activated charcoal to remove Fe, Mn, As and bacteria. The waste generated in the form of slurry can be used as adsorbent to remove As from ground waters in the subsequent remediation processes and it can be regenerated and reused. Problems associated with other remediation processes such as clogging and bacterial growth on adsorbent have been solved by using a specially designed sand filter, which can be maintained at the house. The iron removal process has been demonstrated on site at a village in Assam where iron levels are high (20- 40  $\mu\text{g/ml}$ ). The developed arsenic remediation process has been applied to 10 water samples containing As (100- 750  $\text{ng/ml}$ ) collected at North 24 Parganas and Nadia districts of West Bengal.

For the problem of fluoride toxicity, detection and remediation approach have been applied. With the

help of fluoride detection reagent developed at CCCM/BARC any person can locate safe, less toxic (1.5- 3  $\mu\text{g/ml}$ ) or more toxic water source in their vicinity. By using safe or less toxic water people can save themselves from the harmful effects of fluoride. In this way more than 70% of the problem can be solved with a very little expenditure. For the remediation of more toxic water, slurry of hydrated cerium hydroxide has been used which removes fluoride without contaminating water. Main advantage of this procedure is, higher capacity which is nearly 10 times more than that of alumina and the adsorbent can be regenerated.

The problems associated with respect to contamination, detection and remediation of arsenic, iron, manganese and bacteria are mentioned below.

## Arsenic

Arsenic in groundwater is a global problem. Among the 21 countries facing the problem, Bangladesh and West Bengal are the worst affected. Due to this crisis 136 million people around the world are at

risk. WHO calls it “the largest mass poisoning of a population in history”. Apart from West Bengal and North Eastern States, the other states affected in India are Bihar and Jharkhand. The contamination is spreading very fast to other areas.

In order to solve this problem, two approaches are needed i) Detection by a good detection method which helps in selecting an alternative source of safe water. It also facilitates periodic monitoring of arsenic as the level of arsenic varies from time to time. Presently the detection is being carried out by an expensive visual detection kit which needs to be operated by skilled personnel ii) Remediation by a simpler method, that enables people to prepare arsenic-free water, in the absence of safe alternative source. Moreover the presence of iron in water, facilitates the growth of bacteria which also needs remedial measures.

Several household remediation procedures are being adopted in the affected areas. The main problems associated with these procedures are inefficient removal of arsenic, clogging due to the presence of particles, generation of bacteria in the filtration unit and toxic waste disposal. Some of the most widely used methods are Passive sedimentation (bashi pani), Kolshi filter and bucket treatment unit. The bashi pani is prepared by keeping ground water as collected for 2-3 days before drinking. In this method arsenic removal is partial as it depends on the iron concentration in water. The Kolshi filter consists of layers of Iron, brick, sand and charcoal through which contaminated water is passed and the filtrate is used for drinking. Though the arsenic removal is efficient, the above mentioned problems are still not solved. Bucket treatment unit process lacks proper optimization of oxidant leading to irreproducible results. To solve these problems, slurry of hydrated ferric hydroxide in presence of a powerful oxidant is used, for the oxidation and adsorption of arsenic. The quantity of slurry increases during remediation process due to the presence of iron and manganese in water, which increases the capacity

of slurry. Oxidant is potassium permanganate which is a powerful oxidant and very efficient in the oxidation of arsenic and also in killing bacteria. Due to the colour of potassium permanganate, the end point can be visualised very easily. The process produces toxic waste slurry containing ferric hydroxide and manganese dioxide on which arsenic is adsorbed in the first stage and nontoxic activated carbon slurry waste in the second stage. The toxic waste slurry can be regenerated by alkali treatment and reused in the water treatment. Arsenic from alkali extract can be recovered as ferric arsenate. The process can be scaled up to community and industrial levels too. The proposed water purification system is shown in Fig. 1. The process has been used in the remediation of arsenic from ground waters collected at North 24 Pargana and Nadiya Districts of West Bengal. Results are shown in Table 1.

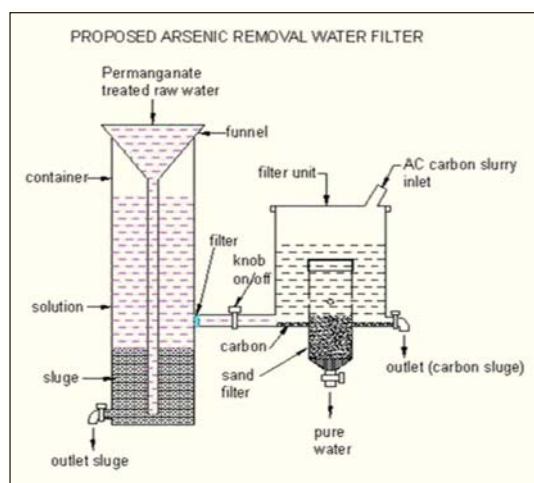


Fig. 1: Arsenic remediation system

Apart from the remediation of the above mentioned elements, detoxification of sulphide, sulphite, nitrite, organic mercury and several organic substances by permanganate treatment, co-precipitation of phosphate and several hydrolysable elements on adsorbent, adsorption of heavy elements like cadmium and mercury and several organic substances on activated charcoal/sand filter were observed which makes the process more dynamic.



Table 1: Analysis of ground waters of West Bengal before and after remediation

Sample	pH	Concentration of As (ng/mL)		Concentration of Fe (µg/mL)		Concentration Mn (µg/mL)	
		Before treatment	After treatment	Before treatment	After treatment	Before treatment	After treatment
1	7.0	750	<10	7.7	<0.1	0.09	<0.05
2	7.1	107	<10	2.6	<0.1	0.40	<0.05
3	6.9	475	<10	1.2	<0.1	0.25	<0.05
4	7.0	250	<10	5.0	<0.1	0.06	<0.05
5	6.9	291	<10	2.1	<0.1	0.14	<0.05
6	7.1	91	<10	3.0	<0.1	0.17	<0.05
7	6.8	200	<10	2.6	<0.1	0.37	<0.05
8	7.0	70	<10	0.6	<0.1	0.07	<0.05
9	7.4	187	<10	1.9	<0.1	0.07	<0.05
10	7.4	265	<10	0.6	<0.1	0.06	<0.05

### Proposed Arsenic remediation procedure

The system developed is very simple consisting of a slurry container, an activated charcoal treatment unit and a sand filtration unit. Its operation is very simple and can be maintained at the house by any one.

The contaminated water is treated with drop-wise addition of  $KMnO_4$  solution till a pink coloured solution is obtained. The pink coloured water is transferred in to the slurry chamber where it is mixed with slurry adsorbent already present in the chamber. The slurry adsorbent is prepared by the oxidation of iron with  $KMnO_4$  and transferred into the slurry chamber. After one hour, the slurry will settle down. The clear pink solution is passed in to the activated charcoal treatment unit where it will be decolourised due reaction with activated charcoal which is then filtered through a sand filter to obtain clear drinking water as per WHO specifications.

The capacity of adsorbent is very high for arsenic. A 30 gm adsorbent can produce 5000 litres of water for a feed water containing 200 ng/ ml of As and no iron. However, for a feed water containing around 10 mg/ mL of iron and up to 2 mg/ ml of As, the capacity of adsorbent is unlimited due to the *in situ*

generation of iron based slurry.

### Iron

Iron in ground water is also one of the major problems in North Eastern States and West Bengal. Iron coexists with arsenic. The presence of iron in water beyond the WHO limit, affects taste/appearance and has adverse effect on domestic use, water supply structures, and promotes iron bacterial growth. Detection of iron is very simple as it can be detected by the colour of red mud precipitate settled at the bottom of water storage containers.



Fig. 2: Ground water containing 40 µg/mL of iron

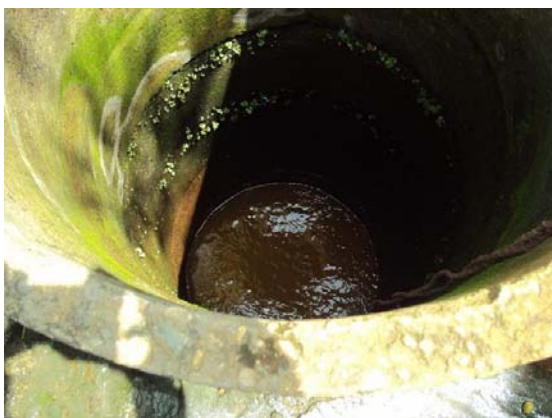


Fig. 3: Iron enriched open well water



Fig. 4: Existing filtration systems for remediation of iron at Monojili village, Tejpur, Assam



Fig. 5: Demonstration of remediation of iron in ground water to the villagers

Remediation of small concentration of iron at 1- 5  $\mu\text{g}/\text{ml}$  is not a big problem and it can be removed by traditional sand filter and also by areal

oxidation. However, higher concentration of iron ( $> 10 \mu\text{g}/\text{ml}$ ) creates severe clogging (due to the precipitation of ferric hydroxide) of open well water source and also sand filter. Some photographs of waters at Monojili village of Assam are show in Figs. 2- 5. At Monojili, all sources of water contain 20- 40  $\mu\text{g}/\text{ml}$  of iron, which is not suitable for domestic purposes. The procedure proposed for arsenic remediation also removes iron which can be used for drinking. However, for the domestic purpose, the above procedure need not be applied due to higher cost and lower yield. To solve this problem, the pink colour water after treatment with  $\text{KMnO}_4$ , can be decolourised with contaminated ground water and filtered through normal sand filter which can be used for domestic purpose. Waste generated [ $\text{Fe}(\text{OH})_3 + \text{MnO}_2$ ] in this process, can be used for water treatment which can fetch some income to the villagers. So the ground water iron which is a curse to the people like Monajili village may be converted as a boon with this value added product. Samples at different villages have been collected and the remediation process was demonstrated to the villagers and a local NGO recommended by BARC. The analysis of waters collected at different places in Assam is given in Tables 2 and 3.

## pH

The ground waters of North Eastern states as well as Nepal and Bhutan are acidic in nature with pH in the range 4-6 while the normal range for drinking water is 6.5- 8.5. Beyond the normal range of pH, the consumption of water will affect the mucus membrane/or water supply system. It can be detected with the help of universal indicator. It can be brought down to normal range (without bacterial contamination) by the addition of sodium bi carbonate. Addition of excess of bicarbonate will not increase pH beyond 8.0 because of buffering action. However, pH is also brought to normal range by the filtration using traditional sand filter but with the risk of bacterial contamination.

Table 2: Assam ground water analysis

Element	1A	2A	3A	4A	5A	6A	7A	8A	9A	10A	11A	12A	13A	14A	15A	16A	17A	18A	19A	20A	WHO limit
pH	6.1	6.3	5.9	6.3	6.3	6.4	6.0	6.2	5.9	5.1	6.2	7.4	7.3	6.9	7.1	6.3	6.9	6.3	6.4	5.9	6.5-8.5*
As(ppb)	<10	<10	<10	<10	<10	<10	<10	<10	<10	21	21	<10	<10	<10	45	<10	<10	<10	<10	<10	10
F-	<1.0	<1.0	<1.0	<1.0	<1.0	<1.0	<1.0	<1.0	<1.0	<1.0	<1.0	<1.0	<1.0	<1.0	3.0	3.0	<1.0	<1.0	<1.0	<1.0	1.5
Fe	4.8	0.2	0.4	0.3	30.6	0.2	17.1	4.4	15.1	24.5	2.7	2.5	2.4	1.2	2.8	11.3	0.3	0.3	<0.01	0.2	0.3
Zn	0.06	<0.05	<0.05	<0.05	<0.05	<0.05	<0.05	<0.05	<0.05	<0.05	<0.05	<0.05	<0.05	<0.05	0.09	<0.05	<0.05	<0.05	<0.05	<0.05	3.0
P	<0.5	<0.5	<0.5	<0.5	<0.5	<0.5	<0.5	<0.5	<0.5	<0.5	<0.5	<0.5	<0.5	<0.5	<0.5	<0.5	<0.5	<0.5	<0.5	<0.5	0.01
Si	22.7	14.5	15.5	20.3	3.7	8.5	5.2	6.4	6.1	6.7	21.2	13.6	11.9	3.0	10.8	24.2	9.0	9.7	13.2	12.2	--
Mn	0.35	0.23	0.50	0.42	0.78	0.27	0.08	0.78	0.62	1.06	0.39	0.03	<0.01	<0.01	0.15	0.06	<0.01	<0.01	0.18	<0.01	0.5
Mg	2.1	10.0	3.4	3.7	15.5	8.4	3.9	16.3	15.5	4.9	3.0	14.3	14.3	2.8	3.9	5.1	4.3	4.6	20.8	4.2	30*
Cu	<0.05	<0.05	<0.05	<0.05	<0.05	<0.05	<0.05	<0.05	<0.05	<0.05	<0.05	<0.05	<0.05	<0.05	<0.05	<0.05	<0.05	<0.05	<0.05	<0.05	2.0
Ti	<0.01	<0.01	<0.01	<0.01	<0.01	<0.01	<0.01	<0.01	<0.01	<0.01	0.13	<0.01	<0.01	<0.01	<0.01	<0.01	<0.01	<0.01	<0.01	<0.01	--
Cr	<0.01	<0.01	<0.01	<0.01	<0.01	<0.01	<0.01	<0.01	<0.01	<0.01	<0.01	<0.01	<0.01	<0.01	<0.01	<0.01	<0.01	<0.01	<0.01	<0.01	0.05
Ca	4.8	21.4	5.8	8.2	12.5	12.1	27.0	13.6	27.5	12.7	8.4	30.9	30.2	12.3	6.6	11.7	7.3	7.6	13.6	8.8	75*
Al	<0.1	<0.1	<0.1	<0.1	<0.1	<0.1	<0.1	<0.1	<0.1	0.16	4.5	<0.1	<0.1	<0.1	<0.1	<0.1	<0.1	<0.1	<0.1	<0.1	0.2
Ba	<0.05	<0.05	<0.05	<0.05	0.19	0.11	<0.05	0.12	0.24	0.06	<0.05	<0.05	<0.05	<0.05	0.06	<0.05	<0.05	<0.05	0.06	<0.05	0.3
Na	9.2	18.6	10.3	14.4	50.7	30.8	14.3	34.0	83.8	15.9	9.4	13.2	13.9	6.9	58.3	6.5	2.4	2.5	11.8	10.3	200
K	1.8	1.3	1.5	1.1	131	20.9	7.3	11.2	10.3	2.7	2.7	7.3	7.4	4.9	0.7	33.5	3.0	3.2	2.7	1.0	--

Values are in µg / ml; more than 90% removal of arsenic on spiked samples at 250 µg/ml (5A, 7A, 16A)

Sample code	Location of sample
1A	IIRM Training Centre borewell, Tezpur
2A	Assam tourism corporation guest house
3A	Batabari village, Assam
4A	IIRM Office, Tezpur
5A	Monojili Village tubewell S-1
6A	Nagaon village openwell S-1
7A	Monojili village tubewell S-3
8A	Monojili village tubewell S-4
9A	Monojili village tubewell S-5
10A	Monojili village tubewell S-6

Sample code	Location of sample
11A	Monojili village openwell S-7
12A	Monojili village openwell S-8
13A	Monojili village openwell S-9
14A	Bramha putra river
15A	Karbi Anglong S-1
16A	Karbi Anglong S-2
17A	Akashganga S-1
18A	Akashganga s-2
19A	Nagaon village tubewell S-2
20A	Bamgaon village

**Bacteria**

Bacterial problem in groundwater is generally less due to the adsorption properties of soil. In remediated water it is introduced during the process of filtration. This problem has been solved in the procedure by reducing the carbon content in the sand filter, as wet carbon is a source of bacterial generation. The sand filter is specially designed so as to remove the filter from the assembly and treat the sand with KMnO<sub>4</sub> which also kills the bacteria. In hilly areas, there are a number of surface water sources that are generally contaminated with

bacteria produced from animal and vegetation products. Regular Permanganate/ activated charcoal treatment and use of this filter may prove to be very useful. The addition of bleaching powder also kills bacteria. However, in the absence of visual end point detection, unstable nature of calcium oxychloride and increased pH, bleaching powder treatment may not be suitable at house hold level. In order to test the killing of bacteria by our procedure, bacteria has been generated on the surface of adsorbent and treated with permanganate and the results are shown in Fig. 6. As shown, the bacterial levels have been brought to zero from 4,440/ml.

Table 3: Assam ground water analysis before and after treatment

Element	Location of the sample					
	Monogili village		IIRM Training Centre		Batabari village	
	Before treatment	After treatment	Before treatment	After treatment	Before treatment	After treatment
pH	6.3	7.1	6.1	7.8	5.9	7.6
As (ppb)	<10	<10	<10	<10	<10	<10
F-	< 1.0	< 1.0	< 1.0	< 1.0	< 1.0	< 1.0
Fe	30.6	<0.01	4.8	<0.01	0.4	<0.01
Zn	< 0.05	< 0.05	0.06	< 0.05	< 0.05	< 0.05
P	< 0.5	< 0.5	< 0.5	< 0.5	< 0.5	< 0.5
Si	3.7	5.9	22.7	19.2	15.5	17.8
Mn	0.78	< 0.01	0.35	< 0.01	0.50	< 0.01
Mg	15.5	21.0	2.1	6.9	3.4	6.4
Cu	<0.05	<0.05	<0.05	<0.05	<0.05	<0.05
Ti	<0.01	<0.01	<0.01	<0.01	<0.01	<0.01
Cr	<0.01	<0.01	<0.01	<0.01	<0.01	<0.01
Ca	12.5	28.0	4.8	24.1	5.8	24.6
Al	<0.1	<0.1	<0.1	<0.1	<0.1	<0.1
Ba	0.19	0.29	<0.05	<0.05	<0.05	<0.05
Na	50.7	89.8	9.2	44.8	10.3	53.4
K 1	31	82.4	1.8	3.9	1.5	4.8

Values are in µg / ml

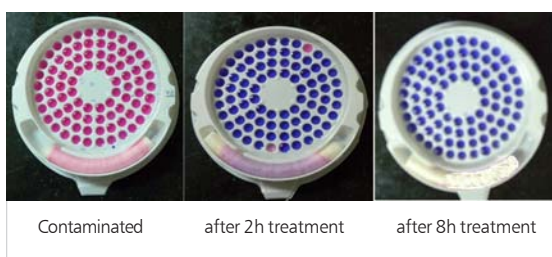
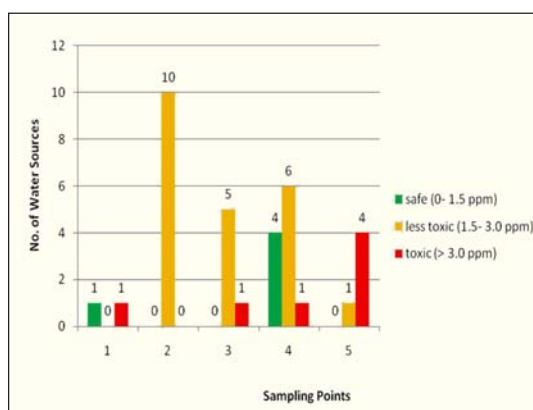


Fig. 6: Bacteria detection before and after KMnO4 treatment (Pink colour is due to bacteria)

### Fluoride in groundwaters

Fluoride in ground water is also a global problem affecting nearly one third of the globe including 21 states in our country. Most of the ground waters of North Eastern States and West Bengal are contaminated with fluoride. The problem can be



1: Vasavi Shiva Nagar Temple 2: Vasavi Shiva Nagar Colony 3: Sonia Nagar 4: Meenakshi Nagar Colony 5: Marrisguda Within 100 metres of radius

Fig. 7: Short range variations of fluoride in waters collected at various places in Hyderabad

solved by searching alternative source available in the vicinity with the help of fluoride detection reagent developed at CCCM (The best reagent among 18 reagents based on a survey conducted by UNICEF). In the absence of a non toxic water source, less contaminated water is the other alternative. USEPA recommends the use of less toxic water (1.5- 3  $\mu\text{g}/\text{mL}$ ) rather than remediation as it causes no serious health problems. This was recommended as short range variations are observed in fluoride concentration in ground waters (Fig. 7). A good house hold detection procedure (CCCM has already developed one) will enable the villagers in finding safer or less contaminated water. In this way, villagers can solve more than 70% of the problem on their own. State Governments can save revenue spent on fluoride remediation projects.

Water containing more than 5  $\mu\text{g}/\text{mL}$  of fluoride is not at all recommended for which remediation is essential. Major problems associated with fluoride remediation are lack of suitable high capacity adsorbent, breakthrough capacity, introduction of salt in remediated water and waste disposal. Most commonly used alumina has problems such as lower capacity, leaching of aluminium, loss of 20% capacity after each cycle of regeneration, need for change of adsorbent after every 4- 5 regenerations

to be predicted based on breakthrough capacity. Nalgonda process based on co precipitation with alum introduces large quantity of salt in water. In order to solve these problems a process has been developed in which slurry of cerium hydroxide is used as adsorbent. It removes fluoride without release of any ion during the remediation process. The main advantage of the adsorbent is its higher capacity (20 mg /g) which is nearly 10 times higher than that of alumina (2.3 mg/g). Every lot of remediated water can be tested with 2- 3 drops of fluoride testing reagent, to monitor the quality of remediation process. Toxic adsorbent can be regenerated and reused for cost effectiveness and waste management. However, like arsenic waste, fluoride waste cannot be treated at home. The process can be made cost effective by using a mixture of rare earth oxides. Further work is in process in this direction.

### **Acknowledgement**

The authors thank Dr. H. Dhattatreya, CEO, IIRM, Tejpur for extending support and local hospitality during sample collected in Assam and Dr. D. Chatterjee, University of Kalyani for help in sample collection at Nadia District, West Bengal.

## DAE-BRNS 11<sup>th</sup> Biennial Trombay Symposium on Radiation & Photochemistry (TSRP-2012): A Report

The 11<sup>th</sup> biennial Trombay Symposium on Radiation & Photochemistry (TSRP-2012) was held at the Training School Hostel, Anushaktinagar, BARC, Mumbai, during January 4 – 7, 2012. This symposium was organized by the Radiation & Photochemistry Division in collaboration with Indian Society for Radiation & Photochemical Sciences (ISRAPS). The symposium was sponsored by the Board of Research in Nuclear Sciences (BRNS). The main objective of this symposium was to discuss the most recent developments in the field of radiation and photochemistry and their applications. About 300 scientists and students both from India and abroad participated in the symposium.

The meeting was inaugurated by Dr. R. K. Sinha, Director, BARC. He spoke about the role of Radiation & Photochemistry in various areas of nuclear energy

programme and released the book of abstracts. Dr. H. N. Ghosh, Convener, TSRP-2012 welcomed the delegates. Dr. T. Mukherjee, Director, Chemistry Group and Chairman, TSRP-2012 spoke about the genesis and importance of Trombay Symposium on Radiation & Photochemistry and released the special issue of ISRAPS Bulletin. Dr. S. K. Sarkar, Head, Radiation & Photochemistry Division and Chairman, Local Organizing Committee, spoke about the contribution of ISRAPS in Radiation and Photochemical Research in BARC and rest of the country. Dr. S. Nath, Secretary, TSRP-2012 proposed the vote of thanks.

Current status and new opportunities in the radiation and photochemical research were discussed in the scientific programme of the symposium including invited talks and contributed papers in the form of



Inaugural address by Dr. R. K. Sinha, Director, BARC. Sitting on the dais (L-R) Dr. S. Nath, Secretary; Dr. T. Mukherjee, Chairman, Symposium Organizing Committee; Dr. S. K. Sarkar, Chairman, Local Organizing Committee; Dr. H. N. Ghosh, Convener, TSRP-2012

poster presentations. A total of forty five invited talks in thirteen sessions by speakers from India as well as abroad and 176 posters in two poster sessions for the contributed papers from the young researchers, including ten posters from abroad, were presented. 32 foreign nationals (USA, Japan, Germany, France, Poland, Russia, Austria) attended the Conference, among them 22 were invited speakers. A special evening session was conducted with talks by Dr. S. Banerjee, Chairman, Atomic Energy Commission, India and Prof. Dr. Helmut Schwarz, President, Alexander von Humboldt Foundation, Germany.

The symposium covered key areas of Radiation & Photochemistry, viz. (a) Ultrafast spectroscopy & dynamics of photoinduced chemical processes, (b) Gas phase reaction dynamics in bulk and beams, (c) Radiation & Photochemistry in nuclear fuel cycle, (d) Radiation and Photochemistry of atmosphere and environment, nanoscale materials as well as biological compounds, antioxidants and drugs, and (e) Industrial and societal applications of radiation and photochemistry.

An exhibition of lasers, optics, detectors and other industrial products was arranged at the symposium venue. Two evening talks by the exhibitors (Andor and Newport) on recent technological developments were very useful for scientists working in the field of spectroscopy. Seventeen students below the age of 32 were awarded the 'Best Poster Presentation' awards by the ISRAPS including one for Dr. Hari Mohan Award (for the best poster) in Radiation Chemistry. Dr. Himansu Sekhar Biswal of Tata Institute of Fundamental Research, Mumbai, was awarded the 'P. K. Bhattacharya Memorial Award' given by ISRAPS.

In the concluding session, Dr. Jai Pal Mittal, Former Director, Chemistry & Isotope Group, BARC, presented a brief summary of the symposium and expressed satisfaction over the gradual improvement in the quality of the TSRP series of symposia following its inception in the year 1992. This was followed by feedback comments from the invited speakers from abroad as well as from young student participants. ISRAPS also felicitated Dr. T. Mukherjee and Dr. P.N. Bajaj for their lifetime contribution to the growth of radiation and photochemical research in India.



Dr. S. Banerjee, Chairman, Atomic Energy Commission, India and Prof. Dr. Helmut Schwarz, President, Alexander von Humboldt Foundation, Germany, delivering their talks in a special evening session

## Towards Smarter and Greener Flow Measurement and Control: A report of the Global Conference and Exhibition

The IV<sup>th</sup> Global Conference and Exhibition with the theme “Towards smarter and greener flow Measurement and Control” was conducted by the Fluid Control Research Institute (FCRI) at Palakkad, Kerala between 18-20 January, 2012. The event was sponsored by several internationally reputed Corporates in the field of instrumentation. Over 300 delegates from India and abroad participated in this three day event.

The Conference was inaugurated by Shri S.Sundareshan, IAS, Secretary, Ministry of Heavy Industries and Public Enterprises, Govt of India.

There were 20 keynote addresses delivered by prominent personalities from Industry and Research Institutes from countries like USA, Singapore and Oman, amongst others.

79 contributed papers, including six papers from BARC, were presented during the 18 Technical sessions, some of which were chaired by senior officers, Dr. P.K.Vijayan, Head, RED and Dr N.L.Soni,

Head, FPTs, BARC. The papers covered a wide range of topics like Flow metering techniques, Measurements for Custody Transfer of oil, gas, water and exotic petro-products, Primary Standards for process parameters, Meter calibration facilities, International comparisons and domestic traceability, Computer modeling applications in flow meter design, Field experience and case studies, Nano fluid technology etc.

An exhibition comprising of 38 stalls was open on all the three days, where both National and International companies displayed a variety of products covering the theme of the Conference.

At the end of the third day, the panel discussion was followed by Valedictory function chaired by Commodore (Retd.) S. Saseendran, Director, FCRI. Based on the audience feedback and appraisal, the contributed paper titled “Performance feedback on cage type control valves used in Heavy Water Application: A case study” from Reactor Group, BARC, co-authored by Shri C. Sengupta and authored and presented by Shri R. Bharathan, was adjudged the Best Technical Paper –Industry (First) and was presented with a Certificate.



Shri R.Bharathan, Head, SRC(M), Reactor Group, presenting the paper.



## DAE-BRNS Symposium on Emerging Trends in Separation Science and Technology (SESTEC-2012): A Report

The fifth DAE-BRNS Symposium on “Emerging Trends in Separation Science and Technology (SESTEC-2012)” was held in SVKM’s Mithibai College, Vile Parle, Mumbai, during February 27 – March 01, 2012. Prof. (Mrs.) Z.R. Turel, Department of Chemistry, Mithibai College, & Convener, Local Organizing Committee (LOC), SESTEC-2012 welcomed the delegates. Prof. Kiran Mangaonkar, Principal, Mithibai College & Chairman, LOC, SESTEC-2012 highlighted different research activities of the host institute and the importance of separation science and technology. Dr. P.K. Mohapatra, Convener, SESTEC-2012 and Head, Actinide

Chemistry Section, Radiochemistry Division, BARC outlined the technical programme of the Symposium and acknowledged the overwhelming response from delegates within the country as well as from overseas. Shri B.P. Sheth, Vice President, SVKM, Vile Parle thanked BARC for accepting their invitation to organize SESTEC-2012 in Mithibai College. Dr. R.K. Sinha, Director, BARC in his inaugural address, highlighted the importance of separation science and technology in the atomic energy programme of India. He made particular mention of the membranes application in different areas of research which are of great importance in different areas like



At the inaugural function from left to right are: Prof. Z.R. Turel, Mithibai College, Mumbai & Convener-LOC, SESTEC-2012, Dr. P.N. Pathak, Secretary, SESTEC-2012, Dr. K. L. Ramakumar, Director, RC&I Group, BARC & Chairman Organizing Committee, SESTEC-2012, Dr. R.K. Sinha, Director, Bhabha Atomic Research Centre, Trombay, Mumbai; Shri B.P. Sheth, Vice President, SVKM, Vile Parle, Mumbai, Prof. Kiran Mangaonkar, Principal, Mithibai College & Chairman-LOC, SESTEC-2012, Dr. P.K. Mohapatra, Convener, SESTEC-2012.

desalination of water and uranium recovery from sea water. He also emphasized the need for forging alliances between academia and research institutes for national benefit. Dr. K.L. Ramakumar, Director, Radiochemistry and Isotope (RC&I) Group, BARC in his Presidential address made special emphasis on the need to develop green technologies to achieve desired separation in different areas of research. The separation technology development should also keep in mind the minimization of waste volume and its treatment to bring about changes to biodegradable form. Dr. P.N. Pathak, Secretary, SESTEC-2012 proposed vote of thanks.

There were about 300 delegates who attended SESTEC-2012 out of which 140 were from DAE including 114 from BARC. It was heartening to note that 214 contributory papers (30 Oral and 184 Poster presentations) in SESTEC-2012 were authored by scientists from 8 National Labs, 24 academic institutions apart from various DAE units. There were 7 plenary and 23 invited speakers (including 13 from overseas) in SESTEC-2012. These speakers were outstanding scientists/technologists and represented 10 countries. All the posters were rapporteured by experts during SESTEC-2012.

A wide range of topics related to separation science and technology were covered including design, synthesis and characterization of solvents and resins, design and development of separation equipment, separation science and technology in the nuclear fuel cycle, emerging separation technologies, electrochemical and pyrochemical separations,

treatment of industrial effluents, isotope separations, membrane science and technology, radiochemical separations, and water treatment and recycling. There was a very lively interaction between the young scholars and the experts during the Poster sessions. Shri T.K. Haldar, Additional Chief Executive, Heavy Water Board, Mumbai delivered a special evening public lecture on "R&D in Separation Science & technology – Contribution to Technology Commercialization" on February 28, 2012.

In the concluding session, a panel discussion was conducted which was chaired by Dr. K.L. Ramakumar, Director, RC&I Group, BARC. Dr. G.D. Jarvinen, Los Alamos National Laboratory, USA, Dr. Isabelle Billard, IPHC/CNRS and Strasbourg University, France, and Dr. (Mrs.) Manjusha Karve, Department of Chemistry, University of Mumbai participated. All the speakers provided their perspective about SESTEC-2012 and on the future directions of separation science and technology. The prizes for best Oral (3) and Poster (15) presentations were also distributed by the Association of Separation Scientists & Technologists (ASSET). A feedback session was arranged to seek suggestions for future programmes. The valedictory function was chaired by Prof. Rajan Welukar, Vice Chancellor, University of Mumbai. Shri S.G. Markandeya, Head, Planning & Coordination Division & Secretary, BRNS emphasized the need for strengthening collaborative research between different DAE units and academic institutions.

## BARC Scientists Honoured

**Name of the Scientist :** Dr. Srikumar Banerjee, Chairman, Atomic Energy Commission & Secretary, Department of Atomic Energy  
**Award :** M.N. Saha Birth Centenary Award  
**Awarded at :** 99<sup>th</sup> Indian Science Congress, KIIT University, Bhubaneswar, India, held during January 3-7, 2012

**Name of the Scientist :** Dr. S. Kailas, Director, Physics Group  
**Award :** C.V. Raman Birth Centenary Award  
**Awarded at :** 99<sup>th</sup> Indian Science Congress, KIIT University, Bhubaneswar, India, held during January 3-7, 2012

**Name of the Scientist :** Dr. Tulsi Mukherjee, Director, Chemistry Group  
**Award :** CRSI Silver Medal (2012) for extensive and outstanding contribution in Chemical Research  
**Awarded by :** Chemical Research Society of India, Bengaluru, at 14<sup>th</sup> CRSI National Symposium in Chemistry at NIIST, Thiruvananthapuram, during Feb. 3-5, 2012

**Name of the Scientist :** Dr. K.B. Sainis, Director, Bio-Medical Group  
**Award :** Lifetime Contribution Award in Free Radical Research  
**Awarded by :** Society for Free Radical Research, India, at SFRR Conference, Kolkata, during Feb.12-14, 2012

**Name of the Scientist :** Dr. P. N. Bajaj, Radiation and Photochemistry Division  
**Award :** Lifetime Contribution Award in Radiation and Photochemical Research  
**Awarded by :** Indian Society for Radiation and Photochemical Sciences at TSRP, Mumbai, during January 4-7, 2012



Birth of Garuda (1987)

Edited & Published by :  
Dr. K. Bhanumurthy,  
Head, Scientific Information Resource Division,  
Bhabha Atomic Research Centre, Trombay, Mumbai 400 085.  
Computer Graphics & Layout : N. Kanagaraj and B.S. Chavan. SIRD, BARC  
BARC Newsletter is also available at URL: <http://www.barc.gov.in>